Severe Faults Accommodation with Formation Reconfiguration in Multi-robot Transportation System

by

Chen Wang
B.Eng., University of Victoria, 2019

A Thesis Submitted in Partial Fulfillment of the
Requirements for the Degree of

MASTER OF APPLIED SCIENCE

in the Department of Mechanical Engineering

© Chen Wang, 2025
University of Victoria

All rights reserved. This thesis may not be reproduced in whole or in part, by photocopying or other means, without the permission of the author.

We acknowledge and respect the Lək̓ʷəŋən (Songhees and Xʷsepsəm/ Esquimalt) Peoples on whose territory the university stands, and the Lək̓ʷəŋən and W̱SÁNEĆ Peoples whose historical relationships with the land continue to this day.

Severe Faults Accommodation with Formation Reconfiguration in Multi-robot Transportation System

by

Chen Wang

B.Eng., University of Victoria, 2019

Supervisory Committee

Dr. Daniela Constantinescu, Supervisor

(Department of Mechanical Engineering)

Dr. Yang Shi, Departmental Member

(Department of Mechanical Engineering)

Dr. Panajotis Agathoklis, Outside Member

(Department of Electrical Engineering)

ABSTRACT

This thesis focuses on handling severe faults in multi-robot transportation systems. It proposes a fault-tolerant framework that integrates optimization models to generate an optimal formation for robots to carry the object for transportation, the Improved Artificial Potential Field (IAPF) method for path planning and motion control, and a proposed strategy of robot cooperation to keep the object balanced all the time.

Multi-Robot Systems (MRSs) offer significant advantages in terms of collaborative intelligence, task expandability, and system reliability. However, addressing severe faults such as motor burnout or structural damage still presents challenges in generating new formations for the remaining healthy robots, as well as reallocating tasks and planning paths during reconfiguration. For MRSs whose mobile robots cooperatively transport an object by supporting it from below, this thesis proposes a path planning framework that ensures that the object reaches the desired destination even when several of the robots fail during transportation. The proposed framework distributes the robots so as to maximize a proposed measure of transportation stability. Specifically, the objective of the constrained optimization that yields the spatial distribution of the robots depends on the distances from the centroid of the object to each robot and to the boundary of the robot formation, with constraints including distribution range, collision avoidance, and the centroid of the object remaining in the convex hull of the robot formation. When faults occur, faulty robots become obstacles, and the same optimization framework generates a new formation for the remaining healthy robots. The Hungarian algorithm serves to construct a distance cost matrix for task reassignment, to minimize the total distance over which the robots move and to reduce energy consumption during reconfiguration.

For path planning and motion control, an IAPF method integrates attractive forces, obstacle and boundary repulsive forces, and a temporary target point strategy

to escape local minima. A collaborative strategy based on half-plane determination and triangular region analysis verifies that the robot formation always includes the centroid of the object in its interior, ensuring that the robots continue to balance the object during reconfiguration. Considering the transportation system a coupled rigid body, IAPF guides its centroid to avoid obstacles and to resume the task.

MATLAB simulations validate the framework across various scenarios in which MRSs with various numbers of robots transport different convex polygonal objects, which, when severe faults happen, need to reconfigure themselves and to resume the transportation while avoiding the failed robots and other obstacles in the environment. Sequential Quadratic Programming (SQP) is applied to solve the optimization problems. Results illustrate that the proposed framework effectively handles severe faults, ensuring continuous and stable transportation tasks. Future work will focus on real-time reconfiguration without task suspension in dynamic environments, constructing a coupled model considering robot and object dynamics, introducing force-feedback collaborative control strategies, and extending to non-holonomic robot scenarios.

Contents

List of Tables

List of Figures

ACKNOWLEDGEMENTS

The successful completion of this research would not have been possible without the support and assistance of many teachers and family members.

First and foremost, I would like to express my heartfelt thanks to my supervisor, Dr. Daniela Constantinescu. From the selection of the research topic to the design of the study, and from the implementations to the writing of this thesis, my supervisor has always provided me with patient guidance and rigorous academic training. In the field of robotics, Dr. Daniela Constantinescu has illuminated the research path for me with profound knowledge, keen academic insight, and a meticulous research attitude, teaching me scientific ways of thinking and research methods. The innovative concepts demonstrated by my supervisor in laboratory management and the freedom given in academic discussions have enabled me to maintain both rigor and creativity throughout the exploration process. Especially during challenging times, my supervisor's careful guidance and encouragement helped me break through bottlenecks, and this sense of gratitude is beyond words.

I would like to thank all the professors at University of Victoria, including Dr. Panajotis Agathoklis, Dr. Wusheng Lu and Dr. Yang Shi, for the professional knowledge they imparted in courses such as Control Theory and Systems, Advanced Engineering Design by Optimization and Advanced Control Theory, which laid a solid theoretical foundation for my research.

I am deeply grateful to my parents who have always been my strongest support. When I was anxious due to research pressure, their understanding and tolerance provided me with warm comfort. I am also grateful to Xiaowei Lu for her support; during the long experimental period, she silently took care of daily chores, allowing me to fully immerse myself in research.

Acronyms

APF Artificial Potential Field.

FTC Fault Tolerant Control.

FTFC Fault Tolerant Formation Control.

IAPF Improved Artificial Potential Field.

MAS Multi-Agent System.

MRS Multi-Robot System.

UAV Unmanned Aerial Vehicle.

UGV Unmanned Ground Vehicle.

Chapter 1

Introduction

1.1 Motivation

Multi-robot systems (MRS) have significant advantages over single robots, such as the comprehensive improvement of collaborative intelligence, task expandability, and system reliability [1]. Through a distributed architecture and dynamic task allocation, multiple robots can overcome their individual physical limitations and achieve efficient collaboration in complex scenarios. For example, multiple welding robotic arms can achieve millimeter-level precision through collaboration in an automobile factory [2]. In agriculture, a cluster of drones equipped with multi-spectral sensors autonomously plan flight routes to accurately identify farmland pests and diseases and targeted pesticide application [3]. The efficiency increases 20 times compared to traditional manual inspections [3]. In the medical field, the Da Vinci surgical multi-robot arm can complete complex operations such as tissue clamping, ultrasonic imaging, and laser cutting simultaneously, significantly improving minimally invasive surgery [4]. In high-risk environments, a redundant number of robots can ensure the continuous operation of the system. For instance, multiple detection robots in a nuclear leakage

site can share radiation data in real time through a self-organizing network. When any robot or its instruments fail, other robots can automatically take over its position [5].

MRSs also exhibit remarkable advantages in object transportation. By dynamically allocating loads and planning paths, they can significantly reduce transportation time, especially when handling large or heavy objects [6]. Besides, MRSs have a high degree of flexibility and environmental adaptability. They are able to adjust their transportation strategies in real-time to deal with obstacles or complex terrains [7]. Moreover, multi-robot cooperation breaks through the load limit of a single robot, allowing the transportation of ultra-large goods through coordinated lifting [8]. MRSs also reduce human intervention, cutting down labor costs in dangerous or repetitive scenarios. In addition, since the robots can operate independently or form collaborative groups, fault tolerant and redundant designs can enable MRSs to continue to work even when a single robot fails, enhancing long-term reliability.

The failures of an individual robot can be categorized as non-severe and severe faults [5]. Non-severe faults include partial malfunctions such as sensor errors, network disconnections, or actuator degradation, where robots retain limited functionality [9]. Severe faults, however, involve catastrophic failures, like motor burnout, battery depletion, or structural damage, which render the robots entirely inoperative [5].

Numerous studies explore how to accommodate the non-severe faults of several robots and to mitigate their impact on the overall mission. A compensation controller is added to the nominal controller of multi-wheeled-mobile robots to effectively eliminate the negative impacts of permanent faults, ensuring the stability of the formation in [10]; a robust adaptive Fault Tolerant Control (FTC) for Multi-Agent System (MAS) with uncertain non-identical dynamics and undetectable actuation

failures simplifies control design and avoids over-estimation in [11]; a novel fault-tolerant formation driving mechanism for heterogeneous Unmanned Ground Vehicle (UGV) is proposed in [12]; a second order MASs controller accommodates actuator failures in a robot team to achieve desired time-varying formations control in [13]; distributed leader-follower fault-tolerant tracking control schemes for a class of high-order nonlinear uncertain MRSs are developed in [14]; a FTC algorithm for MRSs sensor based coverage tasks is proposed in [15]; a comprehensive fault-tolerant framework for MRSs, on robot grouping, task execution, fault detection, and fault tolerance, which allows a team of robots to respond efficiently and quickly to the failure of single or multiple robots is presented in [16]; to avoid the effects of actuator faults on the formation or performance of a robot team as a whole, an active FTC method for second-order multi-agent distributed system with actuator bias faults or the partial loss of effectiveness is proposed in [17]. However, most existing works focus on non-severe faults, and much less work addresses severe faults accommodation.

The strategy to mitigate the severe fault effects on the whole mission requires task re-assignment or team re-formation [5]. Several approaches have been investigated.To reconfigure the formation of the remaining healthy quadrotors and still reach the target point when actuator faults occur in individual Unmanned Aerial Vehicle (UAV), a novel cooperative control reconfiguration scheme with collision avoidance is presented in [18]; to adapt the control law in finite time and maintain the formation geometry, considering actuator failures, such as outage and stuck, a Fault Tolerant Formation Control (FTFC) scheme is designed in [19]; to reconfigure the formation of the remaining health robots using combined Control-Parametrization-and-Time-Discretizations and Generic-Algorithm-Particle-Swarm-Optimization method, an FTFC algorithm for severe actuator faults is developed in [5]. Further related work can be found in [20, 21, 22]. Few existing studies address task reassignment and fault accommodation

by coordination reconfiguration [5]. Generating a new formation and reconfiguring an existing one, including path planing and motion control, remains a challenge.

In multi-robot transportation systems, cooperation plays a significant role. Several researches engage with this topic. To describe the internal force distribution in response to the closed-chain constraints formed by rigid grasping in multi-robot cooperative transportation, realizing dynamic coordination control in multi-robot cooperative transportation, a "macro-mini" structure and a virtual linkage model is proposed in [23]; to integrate both motion coordination tasks (such as formation control) and internal force control during the multi-robot transportation of rigid objects, a two-layer distributed architecture, which uses an observer to estimate the global state and combines adaptive control to handle the dynamic parameter uncertainties of the manipulators in transportation, is proposed in [24]; to improve the collaborative accuracy of multi-robots in complex trajectory tracking tasks, and solve the three-dimensional closed-chain modeling problem, a virtual kinematic chain method for multi-robot cooperative transportation is presented in [25]; to strengthen the stability and adaptability of robots to uneven terrains, a six-degree-of-freedom connector, and with combination of centralized trajectory tracking and decentralized force-guiding control strategies for multi-robot transportation systems are proposed in [26]; for followers to estimate the leader's trajectory through the movement of the object, and to ensure the stability of collaboration based on force feedback and speed compensation, a decentralized controller is proposed in [27]; it is interesting to see that the robots as followers regard the object as a virtual leader to maintain the formation by an asymptotically stable controller from [28]; an extended decentralized control strategy to allow the robots to dynamically adapt to the motion constraints of complex terrains through speed control through a passive sliding mechanism is proposed in [29], and experiments are completed to verify the transportation capability of three tracked

robots in complex terrains; a collaboration strategy that adopts the "steering wheel" collaborative control strategy for object transportation, treating the multi-robot system as an entity with omnidirectional movement ability is presented in [30]; also, the same work [30] proposes a composite connector that integrates passive rotary joints and flexible airbags, so the robot can dynamically adapt to the geometric changes of complex terrains; similarly, robots are simulated as caster mechanisms, adjusting their movements through force sensors without the need for position information, and the speed of each robot is controlled according to the force feedback to achieve collaborative transportation in [31]; by mimicking ant colony behavior, and by using force sensors to dynamically adjust robot trajectories, simulating caster dynamics, with each robot autonomously adjusting its direction solely based on local force feedback to achieve efficient collaborative transportation within complex environments, a multi-robot transportation system based on swarm collaboration is proposed in [32]. However, cooperative robot lifting and balancing of an object for transportation is not yet investigated.

To accommodate severe faults in multi-robot transportation systems, three challenges remain to be addressed:

1. Generating a new formation for the remaining healthy robots to lift and balance the object for transportation

2. Task reassignment, path planning and repositioning control of robots while keeping the object balanced

3. Resuming the transportation with the remaining healthy robots while avoiding collision with the faulty robots and with other obstacles in the environment

Task reassignment is part of the problem to be addressed. Task reassignment assigns each healthy robot to a unique position in the new formation, while minimiz-

ing the distance they travel between their current and their target positions. Several existing algorithms have been investigated for task reassignment. The Hungarian algorithm is designed to solve the assignment problem of minimum or maximum weight matching for bipartite structures, where each matching is a one-to-one correspondence between the two sets [33, 34], and typically, it is applied when searching for global optimal solutions, such as during task allocation and resource scheduling [35]. The global optimal solution is guaranteed in an assignment problem [36, 37], and has a time complexity of $O(n^3)$, which allows efficient handling of medium-scale allocation problems ($n < 100$) [36]. Also, the algorithm has an intuitive logic and is relatively easy to implement [35].The Auction algorithm simulates an auction process where each robot "bids" on positions, iteratively improving the assignment to minimize total cost [38]. It is faster than Hungarian algorithms on large-scale problems in general, but more complex to implement [39]. The Greedy algorithm iteratively assigns the $(\text{Robot}, \text{Position})$ pair with the smallest remaining distance, ensuring no duplicates [40]. It is simple to implement and fast for real-time applications where approximate solutions are acceptable, but the algorithm makes the locally optimal choice (smallest distance) at each step, so an optimal solution is not always guaranteed [40]. Therefore, in this research, the Hungarian algorithm is selected for task reassignment because of its suitability for assignment problem, high computational efficiency, easy implementation and ability to reach the global optimal solution.

An additional challenge when reconfiguring a formation is to reposition the remaining healthy robots while maintaining the object balanced from underneath and avoiding collisions with the faulty peers. Existing work has proposed multiple methods for robots path planning and motion control. Sampling-based algorithms such as Probabilistic Roadmap (PRM) [41] and Rapidly-exploring Random Tree (RRT) [42] are often used to handle the trajectory planning task with high degree of free-

dom configuration. Also, based on the strong duality of convex optimization, the non-differentiable collision constraints are transformed into smooth constraints, and a "least-intrusive" trajectory optimization framework is proposed in [43]. It supports the generation of collision-free or minimum-penetration trajectories for point-mass and full-dimensional objects in scenarios such as autonomous parking, strictly satisfies geometric constraints, and enables real-time optimization, but the algorithm has high computational cost [43]. A Nonlinear Model Predictive Control scheme that consists of learning and query phases is designed in [44]. This method solves the output path tracking problem with input/state constraints (such as a robot tool moving along a geometric curve) without the need to preset time parameters; however, this method depends on an accurate system model [44]. Besides, the current studies widely apply the Artificial Potential Field (APF) method to mobile robots for tasks such as navigating in indoor environments, avoiding obstacles, and reaching a target location [45, 46, 47]. The APF has extremely low computational costs because of the simple mathematical operations based on the gradients of potential functions, and can respond in real-time to changes in a dynamic environment (such as moving obstacles) without having to re-plan the global path [48]. Also, since the APF intuitively simulates a force field, it is simple to implement and easy to expand [48]. Moreover, the trajectories generated by APF are usually continuous and smooth, effectively reducing mechanical stress and improving energy efficiency [49]. In addition, the APF can accommodate multi-robot collaborative control by adding repulsive terms between robots, and supports customization of the potential function to incorporate kinematic/dynamic constraints or to optimize specific objectives [50]. Its main drawback is that it can become trapped in a local minimum when the target point is near an obstacle, making it difficult to reach the destination. The Improved Artificial Potential Field (IAPF) method mitigates the local minimum issue and ad-

dresses a number of other shortcomings of the traditional APF for better adapting to dynamic environments, and improving the accuracy and reliability of path planning [51]. Several interesting results are available in the literature. For highway autonomous driving, an IAPF model that constructs a composite potential field consisting of target, road, lane, vehicle, and velocity potential fields, and optimizes the vehicle speed for safety and comfort, is proposed in [52]; to solve the problems of local minima and vehicle dynamics in dynamic traffic scenarios, for UGV, to achieve natural car-following and lane-changing behaviors, considering vehicle speed and safety distance, an IAPF method is proposed in [53]; to tackle local minima and formation maintenance for the path planning and formation control of multiple UAV in a 3D constrained space, an IAPF method is proposed in [54]. In this research, the IAPF method is adapted to address formation reconfiguration, and is also applied to the entire system to avoid collision with obstacles during transportation.

1.2 Objectives

This thesis proposes a framework for severe fault accommodation in multi-robot transportation systems, that (1) generates an optimal formation and an optimal transportation path for the MRS traveling as a translating rigid body and avoiding obstacles, and (2) generates a new optimal formation with the non-faulty robots and a new optimal transportation path when severe faults occur. As shown in Figure 1.1, the framework comprises four stages.

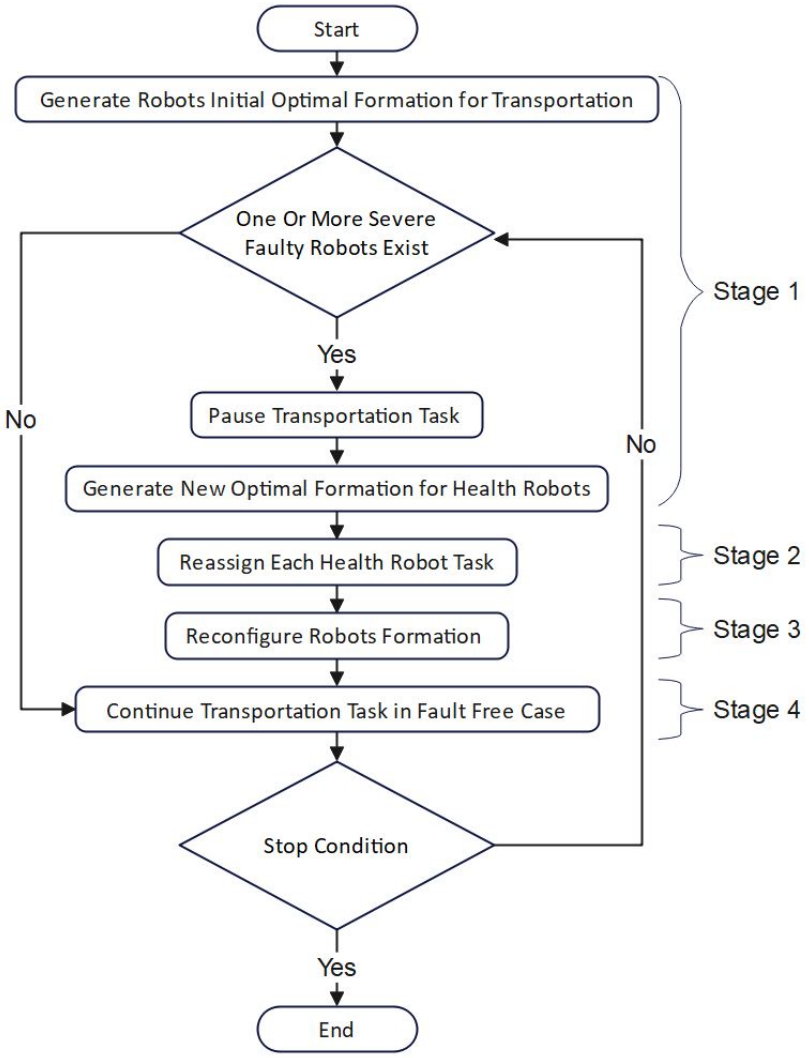

Figure 1.1: Overview of the strategies proposed for severe fault accommodation in MRS transportation

Stage 1 distributes all robots in an optimal convex formation beneath the object, calculated via a proposed stability-maximizing algorithm that balances the center of gravity of the object for transportation. When severely faulty robots are detected, the transportation task pauses, and a new optimal formation is generated for the remaining healthy robots, treating faulty robots as static obstacles.

Stage 2 performs task reassignment. It constructs a cost matrix and applies the

Hungarian algorithm to assign new positions to the remaining healthy robots while minimizing the total traveling distance to ensure energy-efficient reconfiguration.

Stage 3 plans the path and controls the motion of the healthy robots during repositioning. The IAPF method guides the healthy robots to their new positions while keeping their trajectories inside the object boundaries, avoiding collisions and escaping local minima through temporary target points. It also proposes a collaborative repositioning strategy to ensure that the object remains balanced throughout the reconfiguration.

Finally, stage 4 resumes the transportation task with the reconfigured team navigating around faulty robots and environmental obstacles. The IAPF method drives the entire MRS towards the goal position along a collision-free path.

The proposed framework assumes holonomic mobile robots, including omnidirectional platforms equipped with Mecanum wheels or omni-wheels, that can move unrestricted in any direction without reorientation [55] [56].

1.3 Thesis Outline

The thesis is organized as follows:

Chapter 2 models the optimal formation that maximizes a proposed measure of stability of the balance of the object subject to constraints on robot positions, on the centroid of their formation, and arising from the need that the robots avoid collisions among themselves.

Chapter 3 presents a method that treats faulty robots as obstacles and generates a new formation with the healthy robots when some robots suffer severe faults. The Hungarian algorithm reassigns tasks to minimize travel distance, while IAPF enables path planning with escaping from local minima via temporary targets. A collaborative

strategy maintains the object balance during repositioning.

Chapter 4 models the MRS as a coupled rigid body and employs IAPF to provide guidance for obstacle avoidance by combining attractive and repulsive forces with a strategy to select a temporary target to escape local minima, allowing the centroid of the MRS formation to follow safe paths.

Chapter 5 validates the full framework, from initial formation to post-fault task resumption through Matlab simulations. The object is simplified as a 2-D convex polygon, and robots avoid environmental/faulty robot obstacles. Results show that the framework effectively handles severe faults, ensuring successful transportation.

Chapter 6 concludes the thesis and highlights possible future work.

Chapter 2

Initial Optimal Robots Formation Robot Distribution for Object Balance and Transportation

This chapter proposes a method to generate an optimal formation for a multi-robot transportation system. The proposed formation generation technique distributes the robots in a manner that maximizes the stability and the safety of the object during transportation while ensuring that all robots remain within the support area of the bottom surface of the object, that the centroid of their formation coincides with the centroid of the object, and that robots don't collide with each other. A MATLAB simulation validates the proposed initial robot distribution.

2.1 Coordination System

The object for transportation considered in this thesis is a rigid body with uniform thickness and density, and whose top and bottom surfaces are convex polygons. Therefore, the object is simplified as a 2-D convex polygon moving in the horizontal

plane. A fixed reference frame with the origin at a benchmark point in the environment serves to describe all positions of interest. The centroid of the object represents the position of the object in the global frame.

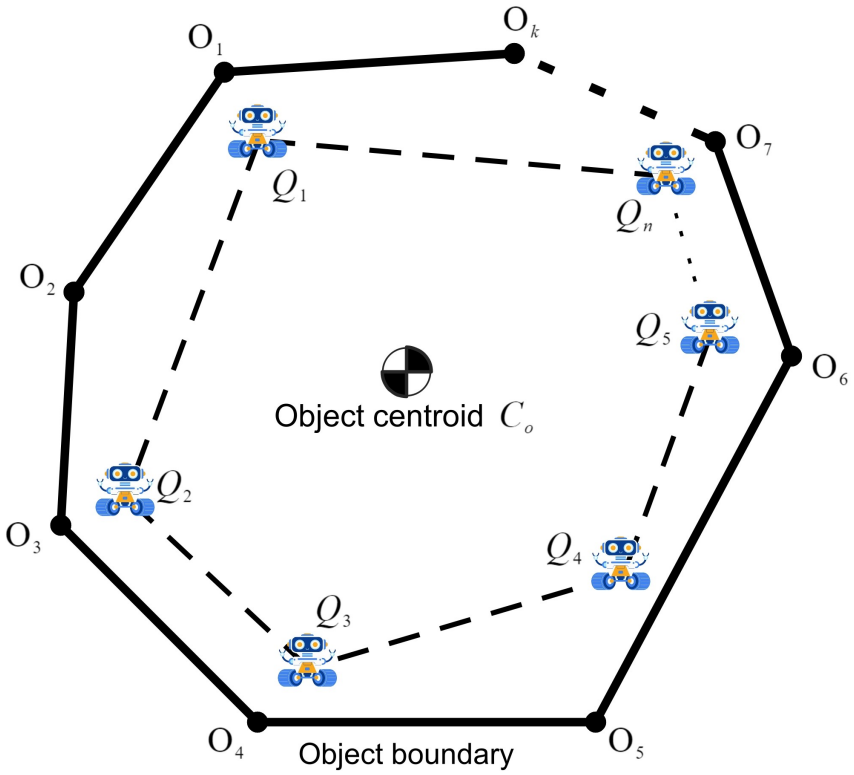

Figure 2.1: Multi-robot transportation system

As shown in Figure 2.1, capital letters represent points in the global coordinate frame. Let a team of mobile robots be assigned for an object transportation task. The configuration of the MRS is denoted as $\mathbf{q} = [\mathbf{q}_1, \mathbf{q}_2, \cdots, \mathbf{q}_n]^\intercal$, and the position of each robot is $\mathbf{q}_i = \begin{pmatrix} q_{x_i} & q_{y_i} \end{pmatrix}^\intercal$, $i \in \{1, 2, \cdots, n\}$. The object is a polygon with k vertices, denoted as $\mathbf{o} = [\mathbf{o}_1, \mathbf{o}_2, \cdots, \mathbf{o}_k]^\intercal$, and each vertex has coordinates $\mathbf{o}_j = \begin{pmatrix} o_{x_j} & o_{y_j} \end{pmatrix}^\intercal$, $j \in \{1, 2, \cdots, k\}$. The centroid of the robot formation is $\mathbf{c}_r = \begin{pmatrix} c_{r_x} & c_{r_y} \end{pmatrix}^\intercal$, and the centroid of the object is $\mathbf{c}_o = \begin{pmatrix} c_{o_x} & c_{o_y} \end{pmatrix}^\intercal$.

2.2 Optimum Robot Distribution

For maximum stability of balancing, the area supported by the MRS should be designed to maximize how difficult it is for the center of gravity of the object to escape it. Each robot provides a support to balance the object, with the centroid of the MRS at or close to the centroid of the object. Therefore, arranging the MRS such that the centroid of the object is as far as possible from each robot and as far as possible from the edges of the robot formation maximizes the stability of the MRS balancing the object. Assuming that the sufficient space is available, the shape of the MRS formation will be a convex polygon.

The objective function is:

$$\underset{\mathbf{q}}{\text{minimize}} \quad -\left(\sum_{i}^{n} d_{ce_i} + \omega \sum_{i}^{n} d_{cq_i}^2\right) \tag{2.1}$$

where d_{ce_j} is the Euclidean distance from the centroid of the object to the edges of the MRS polygon, and d_{cq_i} is the Euclidean distance from the centroid of the object to robot $\mathbf{q}_i$. The ω weight factor is a design parameter.

The distance d_{ce_i} can be obtained from the area of the parallelogram [57]:

$$d_{ce_i} \cdot ||\overrightarrow{Q_iQ_{i+1}}|| = ||\overrightarrow{Q_iQ_{i+1}} \times \overrightarrow{Q_iC_o}|| \tag{2.2}$$

where C_o is the centroid of the object and Q_i and Q_{i+1} are the coordinates of two adjacent robots. Both left and right sides of the Equation (2.2) compute the area of a parallelogram, as shown in Figure 2.2.

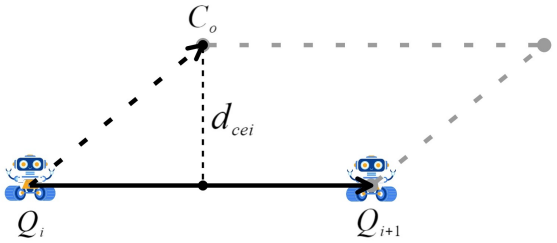

Figure 2.2: Euclidean distance d_{ce_i}

From Equation (2.2), d_{ce_i} can be calculated by:

$$d_{ce_i} = \frac{||\overrightarrow{Q_iQ_{i+1}} \times \overrightarrow{Q_iC_o}||}{||\overrightarrow{Q_iQ_{i+1}}||} \tag{2.3}$$

Since this thesis assumes that the object is a convex polygon, its centroid can be calculated by [58]:

$$\begin{aligned} c_{o_x} &= \frac{1}{6A}\sum_{j=1}^{k}(o_{x_j} + o_{x_{j+1}})(o_{x_j}o_{y_{j+1}} - o_{x_{j+1}}o_{y_j}) \\ c_{o_y} &= \frac{1}{6A}\sum_{j=1}^{k}(o_{y_j} + o_{y_{j+1}})(o_{x_j}o_{y_{j+1}} - o_{x_{j+1}}o_{y_j}) \end{aligned} \tag{2.4}$$

where A is the area of the convex polygon, given by the Surveyor's area formula [59]:

$$A = \frac{1}{2}\left|\sum_{j=1}^{k}(o_{x_j}o_{y_{j+1}} - o_{x_{j+1}}o_{y_j})\right| \tag{2.5}$$

The distance d_{cq_i} is simply:

$$d_{cq_i} = ||\overrightarrow{C_oQ_i}||, \quad i \in \{1, 2, \cdots, n\} \tag{2.6}$$

For successful transportation, all robots must be under the object to provide support, hence, they must be inside of the object convex polygon. This constraint is formulated using the half-plane method, which permits to compute the half-plane in

which the polygon interior lies [57]. As shown in Figure 2.3, after selecting convex polygons with counter-clockwise orientation, the interior of the polygon is always in the left plane of the vector $\overrightarrow{O_jO_{j+1}}$. If each robot can be kept on the left side of the boundary of the object polygon (with counter-clockwise orientation), then the entire MRS stays inside the object polygon.

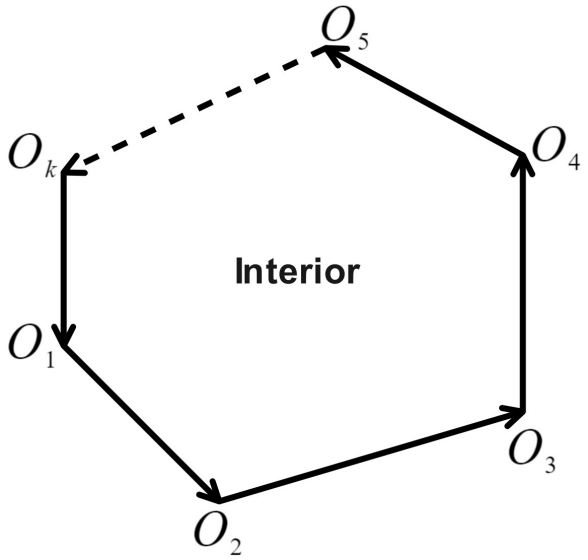

Figure 2.3: Interior of convex polygon with counter-clockwise orientation on the left half plane

The line determined by each side O_jO_{j+1} of the object polygon can be given by the two adjacent vertices:

$$\begin{aligned} a_j x + b_j y + c_j &= 0 \\ a_j &= o_{y_{j+1}} - o_{y_j} \\ b_j &= o_{x_j} - o_{x_{j+1}} \\ c_j &= o_{x_{j+1}} o_{y_j} - o_{x_j} o_{y_{j+1}} \end{aligned} \tag{2.7}$$

where $j \in \{1, 2, \cdots, k\}$. Therefore, after numbering the vertices of the object polygon

counter-clockwise, the constraint on the robot positions is:

$$\mathbf{I}_n \otimes \mathbf{M} \cdot \mathbf{v} \preceq \mathbf{0}, \tag{2.8}$$

where

$$\mathbf{M} = \begin{bmatrix} a_1 & b_1 & c_1 \\ a_2 & b_2 & c_2 \\ \vdots & \vdots & \vdots \\ a_k & b_k & c_k \end{bmatrix} \tag{2.9}$$

$$\mathbf{v} = [\mathbf{q}_1^\intercal \quad 1 \quad \mathbf{q}_2^\intercal \quad 1 \quad \cdots \mathbf{q}_n^\intercal \quad 1]^\intercal$$

and $\mathbf{I}_n \otimes \mathbf{M}$ is the Kronecker product of the n-dimensional identity matrix $\mathbf{I}_n$ and the $\mathbf{M}$ matrix, and $\mathbf{I}_n \otimes \mathbf{M} \cdot \mathbf{v} \preceq \mathbf{0}$ indicates that all entries of the resultant matrix are non-positive.

To avoid overlapping robot positions during distribution, the distance between any two robots should be limited. This constraint is expressed as:

$$d_r - ||\overrightarrow{Q_{i_a} Q_{i_b}}|| \leq 0 \quad \forall i_a, i_b \in \{1, 2 \cdots, n\} \quad \text{and} \quad i_a \neq i_b \tag{2.10}$$

where d_r is the minimum distance allowed between any two arbitrary robots.

For maximally stable support of the object during transportation, the centroid of the MRS formation should coincide with the centroid of the object. Hence, the last constraint is:

$$||\overrightarrow{C_o C_r}|| = 0 \tag{2.11}$$

In summary, the constrained optimization that seeks to maximize the stability of

the object support during transportation is formulated as:

$$\begin{aligned} \underset{\mathbf{q}}{\text{minimize}} \quad & -\left(\sum_{i}^{n} d_{ce_i} + \omega \sum_{i}^{n} d_{cq_i}^2\right) \\ \text{subject to} \quad & \mathbf{I}_n \otimes \mathbf{M} \cdot \mathbf{v} \preceq \mathbf{0} \\ & d_r - ||\overrightarrow{Q_{i_a} Q_{i_b}}|| \leq 0 \quad \forall i_a, i_b \in \{1, 2, \cdots, n\} \quad \text{and} \quad i_a \neq i_b \\ & ||\overrightarrow{C_o C_r}|| = 0 \end{aligned} \tag{2.12}$$

2.3 Implementation and Simulation

This section presents three examples of initial robot optimal formation generation to validate the optimization problem formulated in Section 2.2, for MRSs tasked to transport a convex polygonal object by supporting it from below. A Matlab implementation of the SQP method solves the optimization problem, because of its fast convergence, ability to handle nonlinear constraints and good performance on large-scale problems [60].

Table 2.1 lists the parameter selected for generating the initial optimal MRS formation.

	Parameter	Value
r	- radius of robots	0.1m
v_{max}	- maximum speed of robots	10m/s
d_r	- minimum distance between robots	0.6m
ω	- weight factor	0.5

Table 2.1: Parameters used to determine the initial optimal MRS formation

Figure 2.4 shows an object with fifteen vertices to be transported by a team of twelve robots. Figure 2.5 depicts an object with seven vertices to be transported by a team of six robots. Lastly, Figure 2.6 shows an object with six vertices, to be transported by a team of four robots.

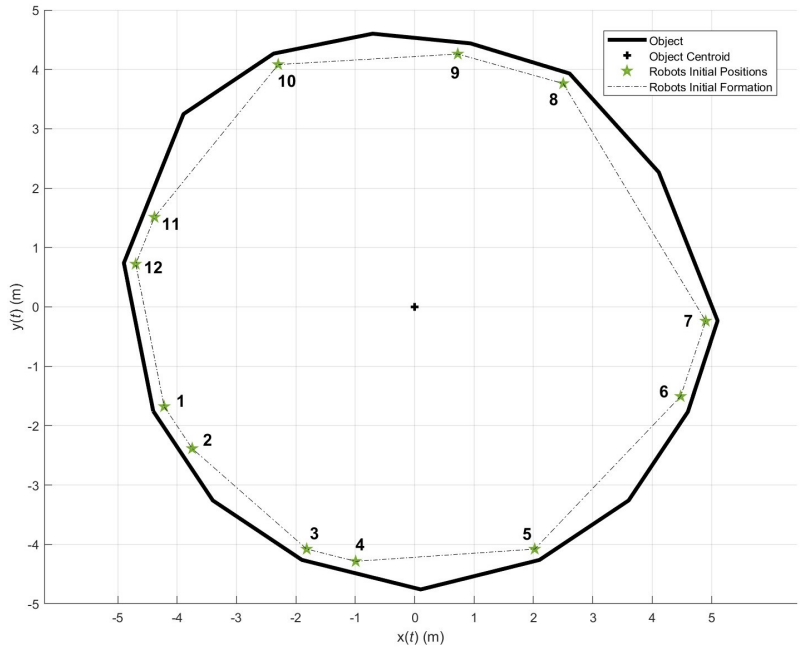

Figure 2.4: Initial optimal formation of a 12 robots MRS transporting a convex object with 15 vertices (a)

In the three simulation examples, the objects have different shapes with different number of vertices, and each transportation task is assigned to a different MRS. The generated initial MRS formations contain the centroid of the object, and all robots are distributed underneath the object they need to support, as far as possible from the centroid of the object. Therefore, the MRS can keep the object balanced during transportation.

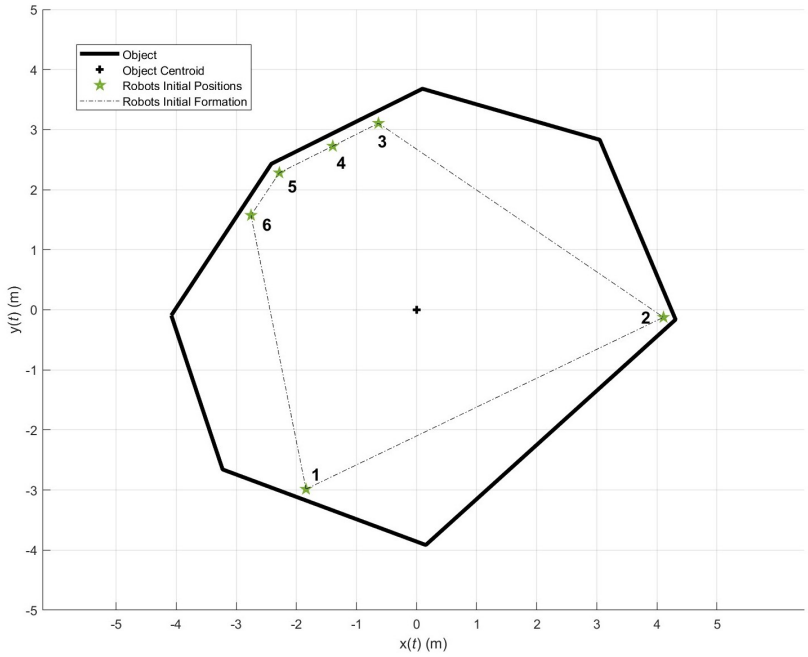

Figure 2.5: Initial optimal formation of a 6 robots MRS transporting a convex object with 7 vertices (b)

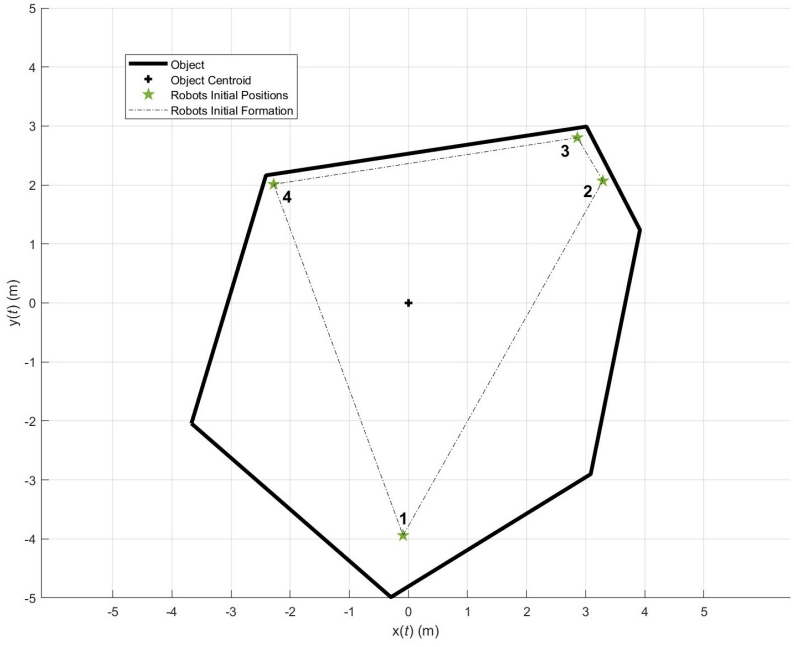

Figure 2.6: Initial optimal formation of a 4 robots MRS transporting a convex object with 6 vertices (c)

2.4 Summary

This chapter has proposed to generate an initial optimal formation for multi-robots cooperatively transporting a convex rigid object. Firstly, the chapter has established the relationship between the centroid of the object and the centroid of the robot formation. Second, the chapter has formulated the computation of the initial MRS formation as a constrained optimization by constructing an objective function that seeks to maximize the distance from the centroid of the object to each robot and to the boundary of the MRS formation, subject to constraints how the robots are distributed under the object, on the distance between any two robots and on the distance between the centroids of the object and of the MRS. Three Matlab simulations, in which the optimization proposed to compute the initial robot formation has been solved using SQP, have illustrated that the proposed optimization yields optimal formations for different MRSs transporting objects with different shapes.

Chapter 3

Formation Reconfiguration due to Severe Faults

During collaborative transportation, when one or more robots suffer severe malfunctions, the remaining healthy robots need to reconfigure their formation to continue to maximize the stability of transportation, ensuring the continuous progress of the task. During the fault-handling process, the transportation task temporarily pauses, and the healthy robots reposition themselves while avoiding collision with the malfunctioning robots and obstacles. The core tasks to generate a new optimal formation are to assign new positions to the remaining healthy robots, and to plan their paths from their current to their new positions while ensuring continuous cooperative balancing of the object.

This chapter tackles the above-mentioned challenges. Firstly, the constrained optimization algorithm from Chapter 2 generates a new formation for the healthy robots, incorporating the positions of malfunctioning robots as obstacle avoidance constraints into the optimization that yielded the initial formation in Chapter 2. Secondly, the Hungarian algorithm assigns robots to new positions, minimizing the

total moving distance during the reconfiguration process. Thirdly, an IAPF algorithm is proposed that plans collision-free paths for all robots that maintain them under the object at all times and escape local minima. Fourthly, a cooperative strategy ensures that the robots maintain the balance of the object while they sequentially reposition themselves. Finally, Matlab simulations verify the effectiveness of the proposed method in different fault scenarios, providing support for fault tolerance in MRS.

3.1 Generation of New Optimal Formation for Healthy Robots

When one or more robots experience severe faults during of transportation, the mission may fail if the team continues to move forward without support from the severely malfunctioning robots. Therefore, the remaining healthy robots need to reconfigure themselves in a new formation that maximizes the stability of object balance during transportation. The transportation mission pauses temporarily for fault accommodation. The generation of a new optimal formation for the remaining healthy robots is similar to the initial optimal formation generation, where the severely malfunctioning robots are treated as obstacles and the remaining healthy robots distribution must be distributed without overlap with the malfunctioning robots.

Let the group of severely faulty robots be $\mathbf{q}_{sf} = [\mathbf{q}_{sf_1}, \mathbf{q}_{sf_2}, \cdots, \mathbf{q}_{sf_m}]^\intercal$, with coordinates $\mathbf{q}_{sf_j} = \begin{pmatrix} x_{sf_j} & y_{sf_j} \end{pmatrix}^\intercal$, $j \leq m$, so the remaining healthy robots are $\mathbf{q}_h = [\mathbf{q}_{h_1}, \mathbf{q}_{h_2}, \cdots, \mathbf{q}_{h_{n-m}}]^\intercal$, with coordinates $\mathbf{q}_{h_i} = \begin{pmatrix} x_{h_i} & y_{h_i} \end{pmatrix}^\intercal$, $i \leq n-m$, and with $n-m \geq 3$, because at least three robots are required to balance the object from the underneath. The new optimal formation for the remaining healthy robots can be generated by the constrained optimization in Equation (2.12), with the additional

constraints:

$$d_r - ||\overrightarrow{Q_{h_i}Q_{sf_j}}|| \leq 0 \quad \forall i \leq n-m \quad \text{and} \quad \forall j \leq m \tag{3.1}$$

where the position of the healthy robot $\mathbf{q}_{h_i} \in \mathbf{q}_h$ is to be optimized, and the severely faulty robot $\mathbf{q}_{sf_j} \in \mathbf{q}_{sf}$ is treated as a static obstacle.

Hence, the constrained optimization function that generates the new positions of the remaining healthy robots becomes:

$$\begin{aligned}
\underset{\mathbf{q}_h}{\text{minimize}} \quad & -\left(\sum_{i}^{n-m} d_{ce_i} + \omega \sum_{i}^{n-m} d_{cq_i}^2\right) \\
\text{subject to} \quad & \mathbf{I}_{n-m} \otimes \mathbf{M} \cdot \mathbf{v}_h \preceq \mathbf{0} \\
& d_r - ||\overrightarrow{Q_{i_a}Q_{i_b}}|| \leq 0, \quad \forall i_a \leq n-m \text{ and } \forall i_b \leq n-m, \text{ with } i_a \neq i_b \\
& d_r - ||\overrightarrow{Q_{h_i}Q_{sf_j}}|| \leq 0, \quad \forall i \leq n-m \text{ and } \forall j \leq m \\
& ||\overrightarrow{C_oC_r}|| = 0
\end{aligned} \tag{3.2}$$

with $\mathbf{v}_h = [\mathbf{q}_{h_1}^\intercal \quad 1 \quad \mathbf{q}_{h_2}^\intercal \quad 1 \cdots \mathbf{q}_{h_{n-m}}^\intercal \quad 1]^\intercal$.

3.2 Remaining Healthy Robots Task Reassignment by Hungarian Algorithm

Once the new optimal formation for the remaining healthy robots is generated, the next step is to re-assign the robots to the new positions. The Hungarian algorithm minimizes the total traveled distance between the current positions of the healthy robots and their desired positions in the new formation, to minimize the energy and time of the reconfiguration process [61]. The cost matrix is provided by the the Euclidean distances from the current positions of the healthy robots to each of the

new positions.

Let the new, optimal positions for the healthy robots be $P_{h_{i'}}$, with coordinates $\mathbf{p}_{h_{i'}} = \begin{pmatrix} x_{h_{i'}} & y_{h_{i'}} \end{pmatrix}^{\mathsf{T}}$. In the cost matrix $\mathbf{C}$, the $c_{h_i h_{i'}}$ entry is then:

$$c_{h_i h_{i'}} = ||\overrightarrow{Q_{h_i} P_{h_{i'}}}||, \quad \forall i, i' \leq n - m, \tag{3.3}$$

each row corresponds to the current position of a healthy robot $\mathbf{q}_{h_i}$ and each column corresponds to a position $\mathbf{p}_{h_{i'}}$ in the new formation. Then, the cost matrix is:

$$\mathbf{C} = \begin{bmatrix} c_{11} & c_{12} & \cdots & c_{1(n-m)} \\ c_{21} & \ddots & & c_{2(n-m)} \\ \vdots & & \ddots & \vdots \\ c_{(n-m)1} & c_{(n-m)2} & \cdots & c_{(n-m)(n-m)} \end{bmatrix} \tag{3.4}$$

and the reassignment problem is solved by minimizing the total distance travelled by all the robots of the MRS by applying the Hungarian Algorithm as follows [62, 63]:

- **Step 1: Cost Matrix Row Reduction**
  1. Find the minimum value in each row of the cost matrix.
  2. Subtract this minimum value from every element in the same row.
- **Step 2: Cost Matrix Column Reduction**
  1. Find the minimum value in each column of the resulting matrix..
  2. Subtract this minimum value from every element in the same column.
- **Step 3: Cover all Zeros with the Minimum Number of Lines in the Cost Matrix**

1. Draw minimum number of horizontal and vertical lines to cover all the zeros in the matrix
2. If the number of lines is equal to the number of rows or columns, identify a set of zeros where each zero is in a distinct row and column. This set corresponds to the minimal total cost assignment.
3. If the number of lines are less than the number of rows or columns, move on to step 4.

- **Step 4: Modify the Cost Matrix**

1. Find the smallest non-covered element by the lines in the matrix, denoted as S.
2. Subtract S from every non-covered element in the matrix.
3. Add S to every element that is covered by two lines to cancel the double subtraction.
4. Then go back to Step 3 and cover all the zeros with the minimum number of lines again.

A critical property of the problem is that addition or subtraction of a constant to all elements in a row or column of the cost matrix, the optimal assignment remains unchanged. The step 1 is to make sure that each row has at least one zero. These zeros are "candidate" assignments where the reduced cost (adjusted cost) is zero, meaning this assignment is as cheap as possible for that robot. Similarly, the step 2 is to ensure each column also has at least one zero. The step 3 is to test if a full optimal assignment (one per row/column) is possible, using graph theory. The zeros in the matrix form a bipartite graph, where robots (rows) and positions (columns) are nodes, and a zero is an edge (possible assignment). According to Konig's Theorem, the number of lines

can represent number of possible assignments, and a "full assignment" is a perfect matching in this graph, exactly one node (robot) matching with one edge (position) without overlaps, so number of lines need to be equal to number of robots/positions. If number of lines are less than it is required, the step 4 is to create new zeros (to expand the candidate assignments) while preserving existing zeros and maintaining the optimality of the solution.

The four steps of the Hungarian algorithm for the cost matrix lead to the assignment with minimum traveling distance for the robots reconfiguration.

3.3 Healthy Robots Reposition Path Planning and Motion Control by IAPF

The transportation pauses when one or more robots experience severe faults, and all robots remain in the current formation until the repositioning of the healthy robots. Additionally, this thesis assumes that: the robots are coupled with the object during transportation; the malfunctioning robots decouple themselves from the object and remain stationary continuing to support it during the repositioning of the healthy robots; the healthy robots also decouple themselves from the object and move under it without friction while repositioning themselves and continuing to support the object. Thus, the severely faulty robots are static obstacles that continue to support the object while the remaining healthy robots reconfigure themselves, and the healthy robots need to avoid collisions with obstacles and with the severely malfunctioning robots. In addition, the environment obstacles are assumed to have lower height than the robots, allowing the object to pass over them. Lastly, while the healthy robots reposition themselves, their paths must remain inside of the object polygon to maintain the object balanced. The IAPF method serves to plan the collision-free

paths for the healthy robots as they reposition themselves in the desired formation while satisfying the object balancing constraints.

The IAPF method creates a virtual potential field around each robot that pushes it toward the target position and pushes it away from obstacles and from the boundaries of the object [64], to avoid collisions with obstacles and keep the object balanced at all times.

Let the desired position of each healthy robot be $\mathbf{q}_{h_{d_i}} = \begin{pmatrix} x_{h_{d_i}} & y_{h_{d_i}} \end{pmatrix}^\intercal$, $i \leq n-m$, the centroid of the object be $\mathbf{c}_o = \begin{pmatrix} c_{o_x} & c_{o_y} \end{pmatrix}^\intercal$, and the position of an obstacle or severely faulty robot be $\mathbf{q}_{obs.h_i} = \begin{pmatrix} x_{obs_i} & y_{obs_i} \end{pmatrix}^\intercal$. During repositioning, the attractive potential field $U_{att.h_i}$ of the goal position is [64]:

$$U_{att.h_i}(\mathbf{q}_{h_i}) = \frac{1}{2} k_{att} \cdot (\mathbf{q}_{h_{d_i}} - \mathbf{q}_{h_i})^\intercal \cdot (\mathbf{q}_{h_{d_i}} - \mathbf{q}_{h_i}) \tag{3.5}$$

where $\mathbf{q}_{h_i}$ and $\mathbf{q}_{h_{d_i}}$ are the current and desired positions of the robot, and k_{att} is the constant of the attractive potential field.

The attractive force $\mathbf{F}_{att.h_i}(\mathbf{q}_{h_i})$ on the robot in the attractive potential field is the negative gradient of $U_{att.h_i}(\mathbf{q}_{h_i})$:

$$\mathbf{F}_{att.h_i}(\mathbf{q}_{h_i}) = -\nabla U_{att.h_i}(\mathbf{q}_{h_i}) = k_{att} \cdot (\mathbf{q}_{h_{d_i}} - \mathbf{q}_{h_i}) \tag{3.6}$$

The repulsive potential field of an obstacle depends on the distance between the robot and the obstacle. Each obstacle has a range within which it repels the robot, ρ_o, the closer the obstacle, the stronger the repulsion. Additionally, the repulsion reduces gradually when the robot approaches the target if the obstacle is nearby the

target. Following [64], the repulsive potential filed is defined as:

$$U_{rep.o.h_i}(\mathbf{q}_{h_i}) = \begin{cases} \frac{1}{2}k_{rep.o}\left(\frac{1}{\rho_{rep.o.h_i}} - \frac{1}{\rho_o}\right)^2 \rho^n_{rep.o.h_i} & \rho_{rep.o.h_i} \leq \rho_o \\ 0 & \rho_{rep.o.h_i} > \rho_o \end{cases} \tag{3.7}$$

where

$$\rho_{rep.o.h_i}(\mathbf{q}_{h_i}) = ||\mathbf{q}_{h_i} - \mathbf{q}_{obs.h_i}|| \tag{3.8}$$

and $\rho_{rep.o.h_i}(\mathbf{q}_{h_i})$ is the distance between the robot and the obstacle; and ρ_o is the range of the repulsive potential of the obstacle, $k_{rep.o}$ is the constant of the repulsive potential field; and n is the IAPF exponent, a positive number. The repulsive force is then given by:

$$\begin{aligned} \mathbf{F}_{rep.o.h_i}(\mathbf{q}_{h_i}) &= -\nabla U_{rep.o.h_i}(\mathbf{q}_{h_i}) \\ &= \begin{cases} \mathbf{F}_{rep.o1.h_i}(\mathbf{q}_{h_i}) + \mathbf{F}_{rep.o2.h_i}(\mathbf{q}_{h_i}) & \rho_{rep.o.h_i} \leq \rho_o \\ 0 & \rho_{rep.o.h_i} > \rho_o \end{cases} \\ \mathbf{F}_{rep.o1.h_i}(\mathbf{q}_{h_i}) &= k_{rep.o}\left(\frac{1}{\rho_{rep.o.h_i}} - \frac{1}{\rho_o}\right)\frac{\rho^n_{att.h_i}}{\rho^2_{rep.o.h_i}} \cdot \frac{\mathbf{q}_{h_i} - \mathbf{q}_{obs.h_i}}{\rho_{rep.o.h_i}(\mathbf{q}_{h_i})} \\ \mathbf{F}_{rep.o2.h_i}(\mathbf{q}_{h_i}) &= \frac{n}{2}k_{rep.o}\left(\frac{1}{\rho_{rep.o.h_i}} - \frac{1}{\rho_o}\right)^2 \rho^{n-1}_{att.h_i} \cdot \frac{\mathbf{q}_{h_{d_i}} - \mathbf{q}_{h_i}}{\rho_{att.h_i}(\mathbf{q}_{h_i})} \end{aligned} \tag{3.9}$$

The repulsive force of the obstacle has two components: $\mathbf{F}_{rep.o1.h_i}$ pushing the robot away from the obstacle, and $\mathbf{F}_{rep.o2.h_i}$ guiding the robot towards the desired position. The $\rho_{att.h_i}(\mathbf{q}_{h_i}) = ||\mathbf{q}_{h_{d_i}} - \mathbf{q}_{h_i}||$ is the distance between the current position and the desired position of the robot

To keep the robots inside the object polygon all the time, another repulsive potential is needed to push them away from the boundaries of the object. Motivated by [52], the repulsive force of the object edges are:

$$
\begin{aligned}
\mathbf{F}_{rep.e.h_i}(\mathbf{q}_{h_i}) &= \begin{cases} \mathbf{F}_{rep.e1.h_i}(\mathbf{q}_{h_i}) + \mathbf{F}_{rep.e2.h_i}(\mathbf{q}_{h_i}) & \rho_{rep.e.h_i} \leq \rho_e \\ 0 & \rho_{rep.e.h_i} > \rho_e \end{cases} \\
\mathbf{F}_{rep.e1.h_i}(\mathbf{q}_{h_i}) &= k_{rep.e}\left(\frac{1}{\rho_{rep.e.h_i}} - \frac{1}{\rho_e}\right)\frac{\rho^n_{att.h_i}}{\rho^2_{rep.e.h_i}} \cdot \frac{\mathbf{c}_o - \mathbf{q}_{h_i}}{||\mathbf{c}_o - \mathbf{q}_{h_i}||} \\
\mathbf{F}_{rep.e2.h_i}(\mathbf{q}_{h_i}) &= \frac{n}{2}k_{rep.e}\left(\frac{1}{\rho_{rep.e.h_i}} - \frac{1}{\rho_e}\right)^2 \rho^{n-1}_{att.h_i} \cdot \frac{\mathbf{q}_{h_{d_i}} - \mathbf{q}_{h_i}}{\rho_{att.h_i}(\mathbf{q}_{h_i})}
\end{aligned}
\tag{3.10}
$$

where $\rho_{rep.e.h_i}(\mathbf{q}_{h_i})$ is the distance from the robot to the closest edge of the object polygon, which can be obtained from Equation (2.3), and ρ_e is the influence range of the repulsive potential field of the edge. Also, $k_{rep.e}$ is the constant of the edge repulsive potential. Similarly to the repulsive forces of the obstacles, $\mathbf{F}_{rep.e1.h_i}$ pushes robots away from the edge to the object centroid, and $\mathbf{F}_{rep.e2.h_i}$ guides the robot to the target, as shown in Figure 3.1.

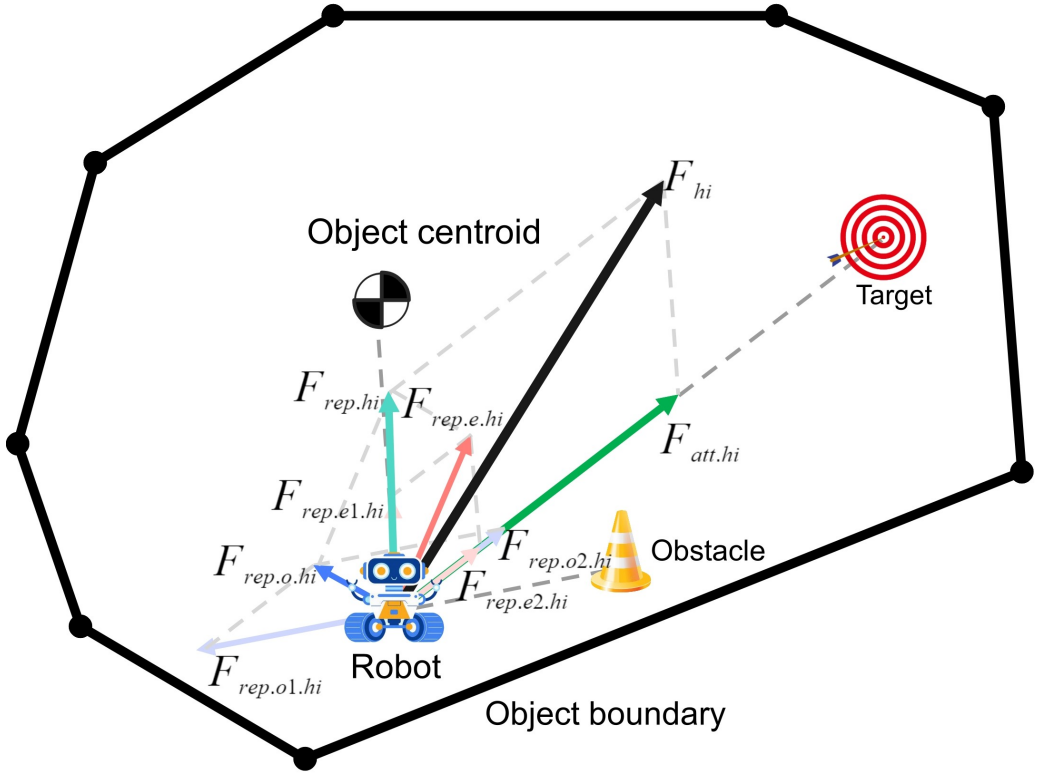

Figure 3.1: Potential forces on a robot in the IAPF potential field

The resultant force $\mathbf{F}_{h_i}(\mathbf{q}_{h_i})$, shown in Figure 3.1, on the robot in the IAPF is then:

$$\mathbf{F}_{h_i}(\mathbf{q}_{h_i}) = \mathbf{F}_{att.h_i}(\mathbf{q}_{h_i}) + \mathbf{F}_{rep.o.h_i}(\mathbf{q}_{h_i}) + \mathbf{F}_{rep.e.h_i}(\mathbf{q}_{h_i}) \tag{3.11}$$

This force provides the velocity command for the robot.

3.4 Escaping from Local Minima using Temporary Target Points

A key drawback of IAPFs obtained from the superposition of several attractive and repulsive potentials is that they have multiple local minima. As a result, a robot may become trapped in a local minimum and not be able to reach its target, as shown in Figure 3.2 and Figure 3.3.

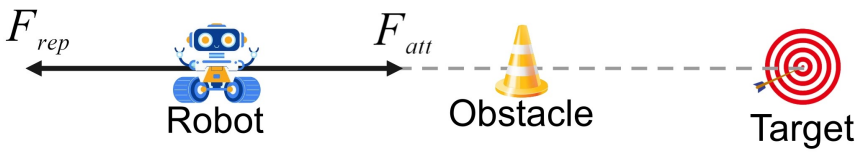

Figure 3.2: IAPF local minimum (a)

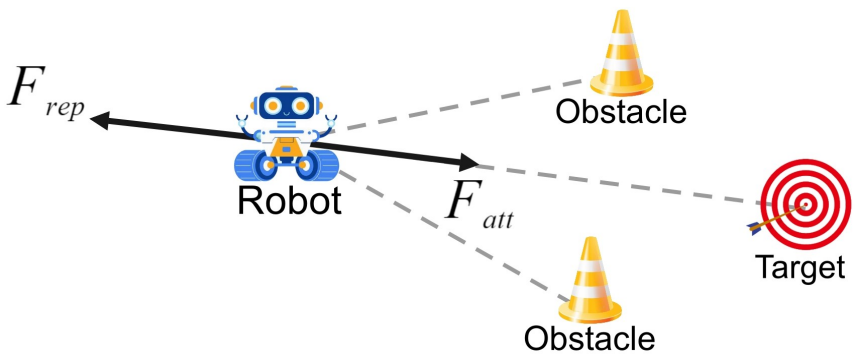

Figure 3.3: IAPF local minimum (b)

As proposed in [65], the robots can escape a local minimum of an IAPF by selecting

a temporary target near the obstacle that causes the local minimum and moving towards it. After reaching the temporary target and escaping the local minimum, the robot can continue to move towards its real target. The four-step strategy is proposed to find a temporary target position for a robot trapped at a local minimum of the IAPF:

- **Step 1: Locating All Involved Obstacles**

  At local minimum the distances between all robots and all obstacles are computed to determine all obstacles with robots in the range of their repulsive fields.

- **Step 2: Locating all Temporary Target Candidates**

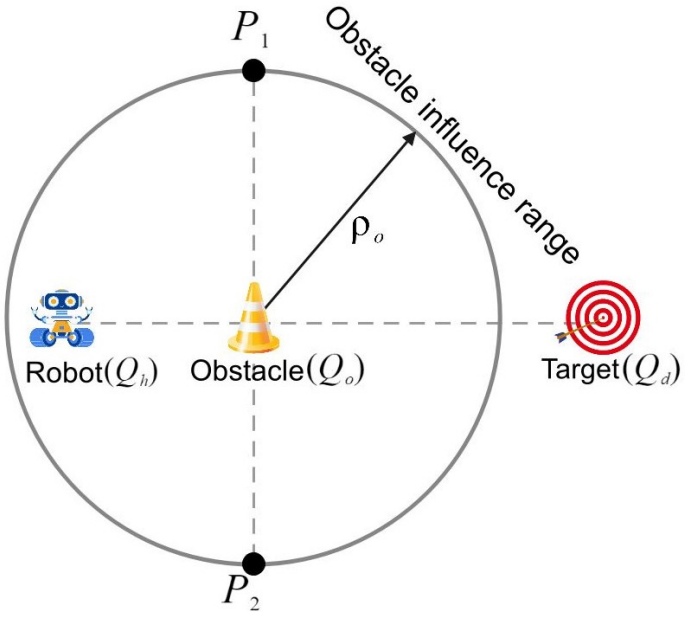

Figure 3.4: Candidate temporary targets, P_1 and P_2

As shown in Figure 3.4, the two candidate temporary targets, P_1 and P_2, are the two end points of the diameter of the range that is perpendicular to the line

from the robot to its target, namely:

$$\begin{aligned} P_1 &= Q_o + \rho_o \hat{\mathbf{u}} \\ P_2 &= Q_o - \rho_o \hat{\mathbf{u}} \end{aligned} \tag{3.12}$$

where, $\hat{\mathbf{u}}$ is the direction perpendicular on $\overrightarrow{Q_h Q_d}$ and can be found by:

$$\hat{\mathbf{u}} = \frac{\overrightarrow{Q_h Q_d}}{||\overrightarrow{Q_h Q_d}||} \cdot \begin{bmatrix} 0 & 1 \\ -1 & 0 \end{bmatrix} \tag{3.13}$$

- **Step 3: Feasible Candidate Temporary Targets**

  Among the candidate temporary targets identified in the previous step, only those inside the object and outside all repulsive potentials are feasible temporary targets.

- **Step 4: Best Temporary Target Position**

  Among the feasible candidate temporary targets, the robot selects the candidate closest to the centroid of the object, to avoid possible minima created by the superposition of the repulsive fields of an obstacle and an object edge.

3.5 Cooperation of MRS to Keep the Object Balanced During Repositioning

During repositioning, the healthy robots need to cooperate with each other to keep the object balanced all the time. The malfunctioning robots provide static supports, and the healthy robots provide moving supports. We propose a repositioning strategy that moves the healthy robots one by one in a manner that permits them to cooperatively balance the object at all times.

Initially, all healthy and malfunctioning robots form a convex polygon that maximizes the stability of the object balance. A robot moving from its current position to a new one affects only the two edges of the MRS formation on which it lies. Let the healthy robot currently repositioning itself be $\mathbf{q}_i \in \mathbf{r}$, with neighbors $\mathbf{q}_{i-1}$ and $\mathbf{q}_{i+1}$. The line passing through its neighbors splits the object polygon into two regions, see Figure 3.5 and Figure 3.6

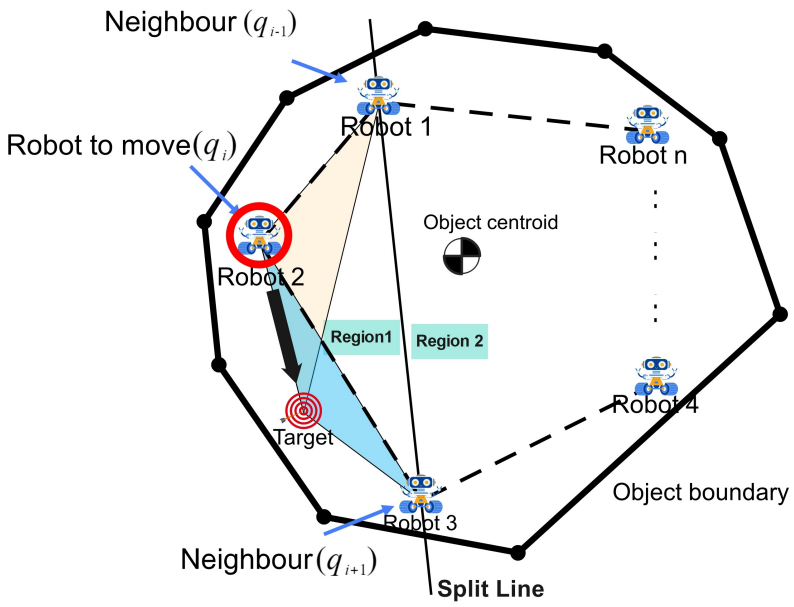

Figure 3.5: Strategy to reposition a healthy robot while keeping the object balanced (a)

If both the current and new positions of the healthy robot $\mathbf{q}_i$ are in the same region, and the centroid of the object is outside of the triangles formed by the current and new positions of the robot with the positions of its neighbors and robot $\mathbf{q}_i$ is feasible to reposition.

If the current and new position of the healthy robot $\mathbf{q}_i$ are in different regions, as shown in Figure 3.6, but the MRS, including the malfunction robots, can keep the object balanced without robot $\mathbf{q}_i$; then, robot $\mathbf{q}_i$ is feasible for repositioning.

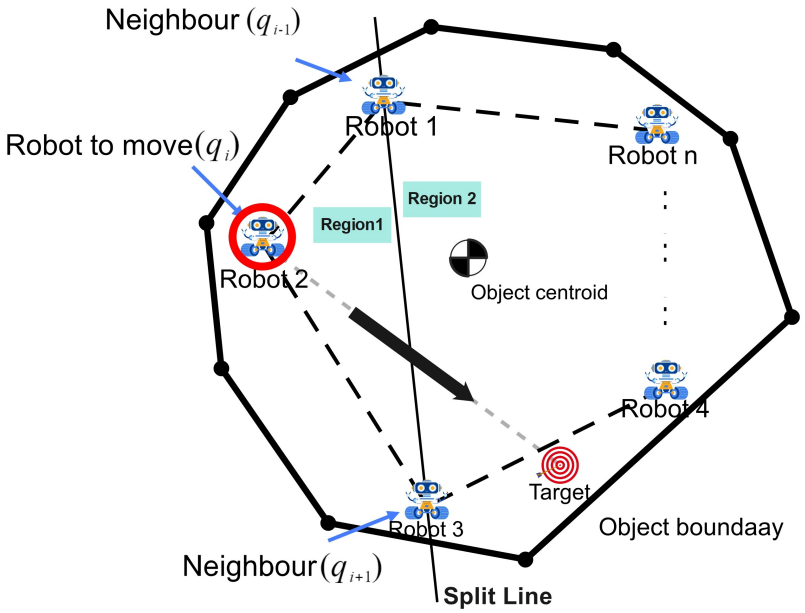

Figure 3.6: Strategy to reposition a healthy robot reposition while keeping the object balanced (b)

If it is not feasible that robot $\mathbf{q}_i$ repositions itself, then robot $\mathbf{q}_{i+1}$ tries to reposition itself, and the process repeats until all robots reposition themselves. Any robot that may not be able to reposition itself given the current MRS formation may be able to do so after the other robots reposition themselves and the MRS formation changes. Although relatively unlikely, it is possible that one or more robots may not be able to reposition themselves after all other robots have reached their new positions, leading to the failure of the MRS transportation mission.

The half plane method from Section 2.2 can be applied again to determine if the current and new positions of robots are in the same region. Given the current robot position $\mathbf{q}_i = \begin{pmatrix} x_i & y_i \end{pmatrix}^\intercal$, its target position $\mathbf{q}_{d_i} = \begin{pmatrix} x_{d_i} & y_{d_i} \end{pmatrix}^\intercal$, the positions of the two neighbors $\mathbf{q}_{i+1} = \begin{pmatrix} x_{i+1} & y_{i+1} \end{pmatrix}^\intercal$ and $\mathbf{q}_{i-1} = \begin{pmatrix} x_{i-1} & y_{i-1} \end{pmatrix}^\intercal$ and the centroid of

the object $\mathbf{c}_o = \begin{pmatrix} c_{o_x} & c_{o_y} \end{pmatrix}^\intercal$, Equation (2.7) can be re-written as:

$$\begin{aligned} \text{sign}_{rob} &= (y_{i+1} - y_{i-1})x_i + (x_{i-1} - x_{i+1})y_i + (x_{i+1}y_{i-1} - x_{i-1}y_{i+1}) \\ \text{sign}_{tar} &= (y_{i+1} - y_{i-1})x_{d_i} + (x_{i-1} - x_{i+1})y_{d_i} + (x_{i+1}y_{i-1} - x_{i-1}y_{i+1}) \end{aligned} \tag{3.14}$$

with $i \leq n - m$. If $\text{sign}_{rob} = \text{sign}_{tar} \neq 0$, the current and new positions of robot $\mathbf{q}_i$ are in the same region; otherwise, they are in the different regions. If $\text{sign}_{rob} = \text{sign}_{tar} = 0$, the current and new positions of robot $\mathbf{q}_i$ are on the split line and the robot can reposition itself because its motion does not change the robot formation. The half plane method also serves to determine if the MRS formation contains the centroid of the object.

3.6 Healthy Robots Cooperative Formation Reconfiguration Strategy

Figure 3.7 summarizes the strategy by which the healthy robots cooperatively reposition by IAPF. When some robots are identified as suffering from severe faults, the MRS pauses the transportation of the object and the repositioning of the remaining healthy robots starts. Namely, a new optimal formation is computed for the remaining healthy robots, and the Hungarian algorithm assigns the new positions to the robots. Then, the robots reposition themselves one by one while cooperatively balancing the object. Several conditions are crucial to a successful formation reconfiguration.

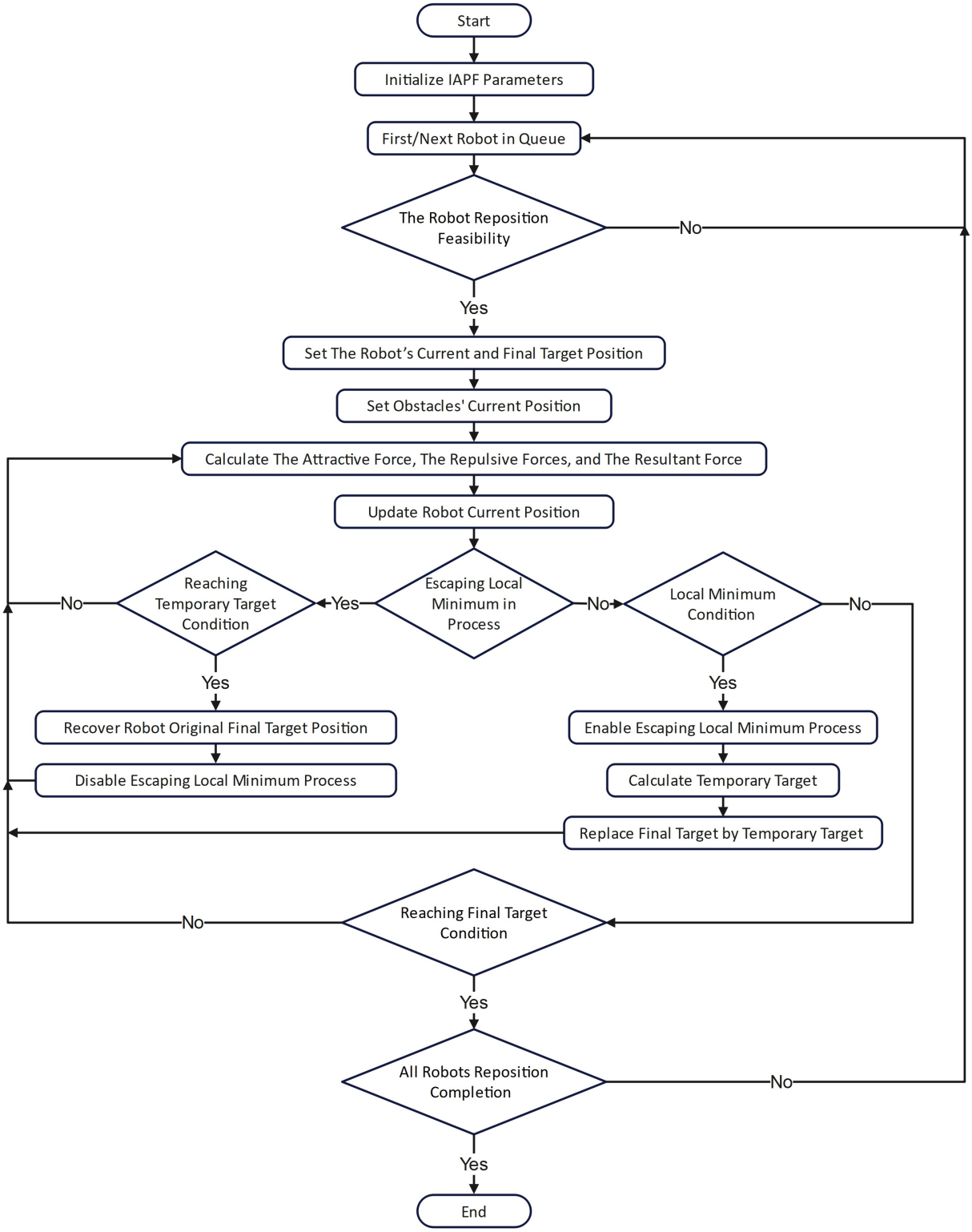

Figure 3.7: Flow chart of the strategy by which the healthy robots reposition themselves one by one while keeping the object balanced

The "local minimum condition" determines whether a robot becomes trapped at a local minimum. The condition measures two factors: the resultant force on the robot and the distance of the robot to its final target position. The robot is trapped at a local minimum if has not reached its final target position, but the resultant force on it is close to zero. Then, to escape the local minimum, the robot selects a temporary target, instead of its original target, and moves towards it.

The "reaching temporary target condition" measures the distance of the robot to the temporary target, which determines if the robot has escaped the local minimum. If the distance is smaller than a pre-selected threshold, the robot has escaped the local minimum, and the temporary target disappears. The robot resumes its motion towards the original final target.

The "reaching final target condition" indicates if the robot has reached its final target position. If the robot is close to its final target point, the robot has finished repositioning, next robot in the queue starts to reposition itself. Once all robots have reached their final target positions, the MRS formation reconfiguration is completed.

3.7 Implementation and Simulation

This section presents three simulation studies to validate the strategy proposed for severe faults accommodation in an MRS transporting a convex polygonal object by supporting it from below. The simulations link to the three simulations which illustrate how the initial optimal formation of the MRS is generated in Section 2.3, to demonstrate various scenarios. Specifically, the numerical examples in this section illustrate the generation of new optimal formation for the healthy robots from Section 3.1, the assignment of new positions to all healthy robots by the Hungarian algorithm from Section 3.2, the successive repositioning of the healthy robots controlled

by the IAPF to satisfy the requirements from Section 3.3: collision avoidance, escape from local minima, and cooperative balancing of the object during the repositioning from Section 3.4. The simulation parameters are shown in Table 3.1.

	Parameter	Value
r	- radius of robots	0.1m
v_{max}	- maximum speed of robots	10m/s
d_r	- minimum distance between robots	0.6m
ω	- weight factor	0.5
k_{att}	- constant of the attractive potential	6
$k_{rep,o}$	- constant of the repulsive potential of the obstacle	1
ρ_o	- range of repulsive potential of the obstacle	0.8m
ρ_c	- obstacle collision range (radius)	0.3m
$k_{rep,e}$	- constant of the potential foeld of the object edges	0.5
ρ_e	- range of the repulsive potential of the object edges	0.2m
n	- IAPF exponent [64]	2

Table 3.1: Healthy robot formation reconfiguration IAPF parameters

Simulation Example 1

In Figure 3.8, the object has fifteen vertices, and its transportation is assigned to an MRS with twelve robots with the initial formation computed in Section 2.3. During transportation, six robots (1, 3, 5, 6, 8, 10, shown in Figure 3.8 as black circles) experience severe faults and are treated as static obstacles during formation reconfiguration. The transportation pauses for the faults accommodation. The static environment obstacles A, B and C have the same dimension as the robots. As in the algorithm that computes the initial optimal formation for the entire MRS, SQP is used to solve Equation (3.2) to determine the new optimal formation for the remaining

six healthy robots. Then, the Hungarian algorithm assigns the new positions to the healthy robots, as discussed in Section 3.2 , to minimize the total distance traveled by all healthy robots, so each robot has a unique target position for reconfiguration.

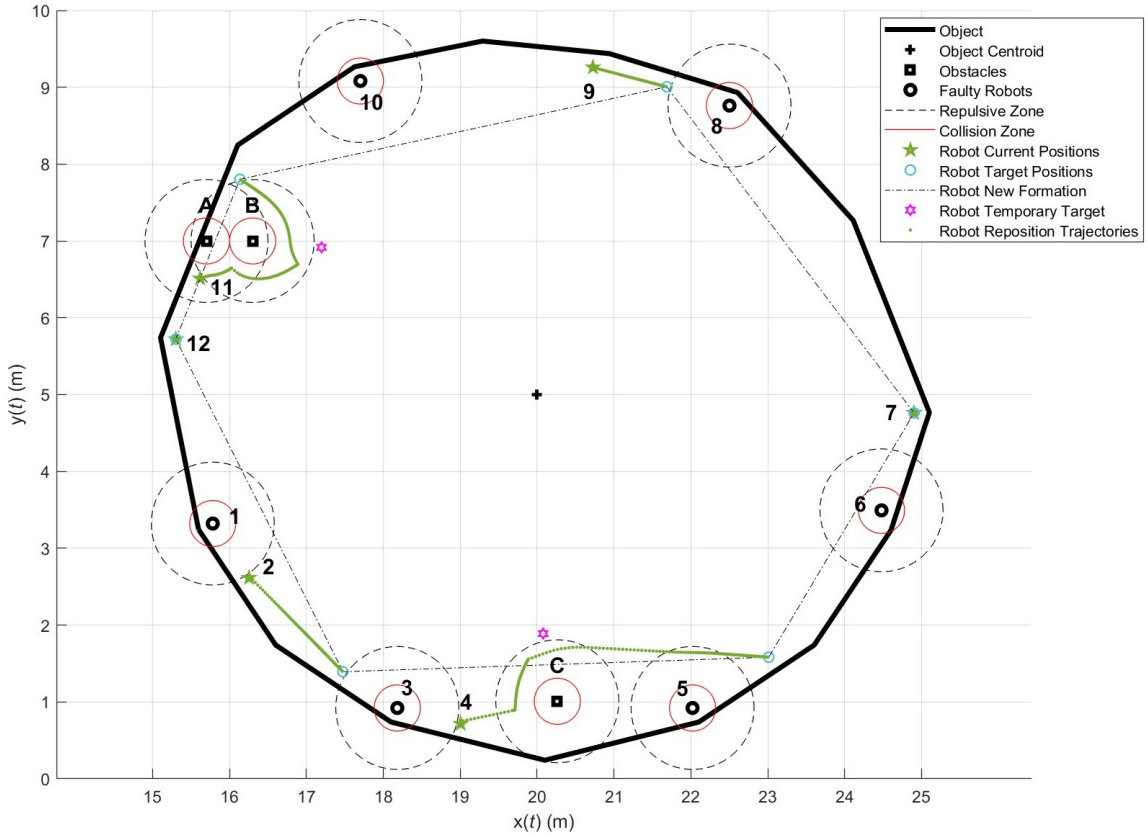

Figure 3.8: Formation reconfiguration for the remaining six healthy robots of an MRS with twelve robots suffering from severe faults (a)

Robots 7 and 12 are not assigned new positions during repositioning, so they do not need to move. Also, robots 2 and 9 move directly towards their targets because no malfunctioning robots or obstacles are in their way.

Obstacle C is on the path of robot 4 to its target and traps the robot into a local minimum of its IAPF, similarly to the scenario in Figure 3.2 in Section 3.4. Therefore, robot 4 uses the four steps algorithm proposed in Section 3.4 to identify a temporary target to escape the local minimum before resuming its travel towards its original

target position.

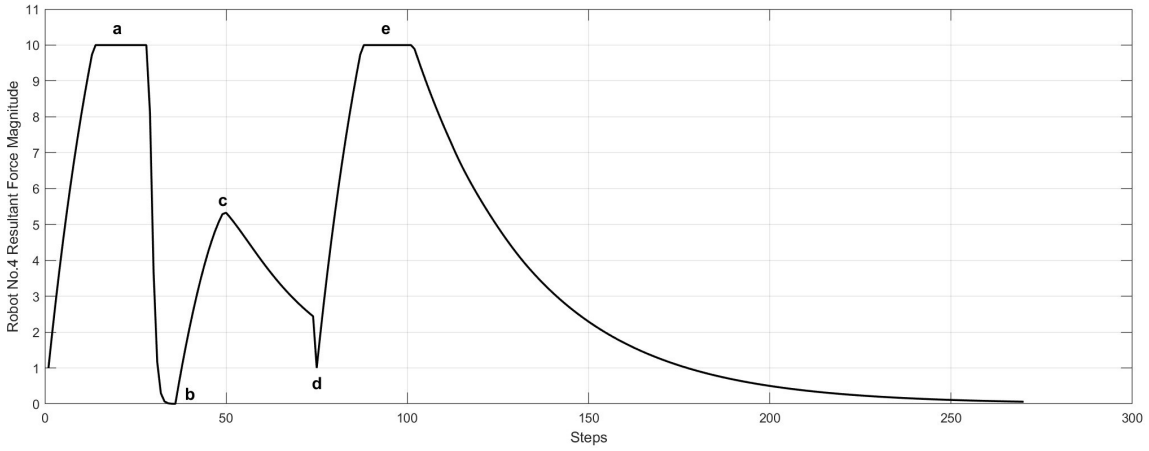

Figure 3.9: The resultant control force on robot 4

The resultant control force on robot 4 is shown in Figure 3.9. The force grows to the maximum value before the robot enters the repulsive field of the obstacle; then, the force decreases abruptly to zero when the robot is inside the repulsive field of the obstacle, at b in Figure 3.9, when it gets trapped in the local minimum. After the robot selects a temporary target, its control force increases to c, and guides the robot away from the local minimum. The force decreases to d when the robot approaches its temporary target; then, the robot aborts the temporary target in favor of its original final target, and the resultant force increases to e and decreases gradually when it approaches its final target.

Obstacles A and B cause a local minimum along the path of robot 11, similarly to the scenario introduced in Figure 3.3 from Section 3.4. The robot finds a temporary target to escape the local minimum, and successfully reaches the target position.

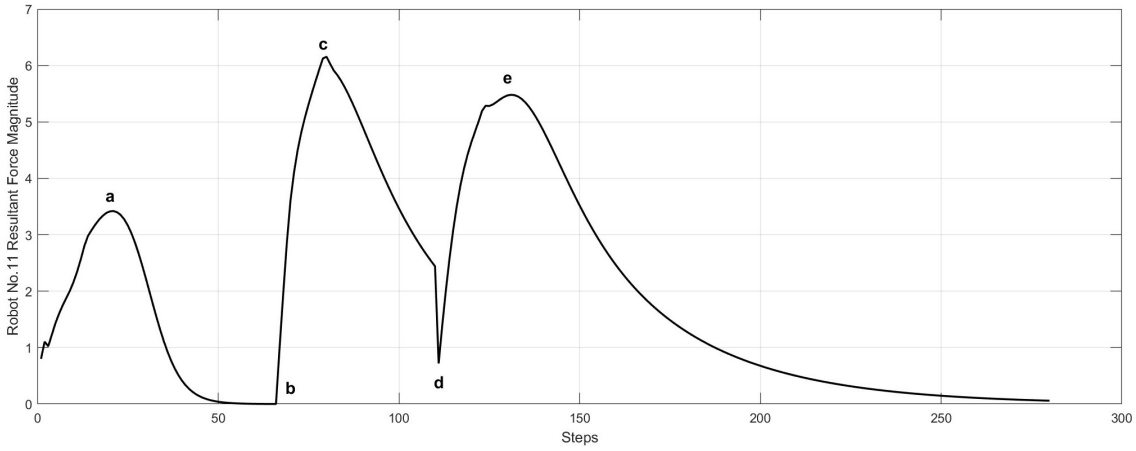

Figure 3.10: The resultant control force on robot 11

The resultant control force on robot 11 is shown in Figure 3.10. Initially, two obstacles repel the robot, and the resultant force fluctuates and gradually decreases to zero, at b, when the robot becomes trapped in a local minimum. The resultant force increases to c when the robot selects a temporary target, which guides it escaping from the local minimum. The force reduces to d and increases dramatically to e when the robot finishes its escape from the local minimum; then, the resultant force guides the robot towards its final target.

Simulation Example 2

In Figure 3.11, the object has seven vertices, and its transportation is assigned to a team of six robots initially. Robots 3 and 4 suffer severe faults, and become static obstacles, as shown in the Figure 3.11 through the black circles. The environment obstacles A and B have the same dimensions as the robots. The transportation pauses for faults accommodation. A new optimal formation is generated and assigned to the remaining four healthy robots. While repositioning by IAPF, robots are prevented from crossing the object boundary by the repulsive potential of the boundary.

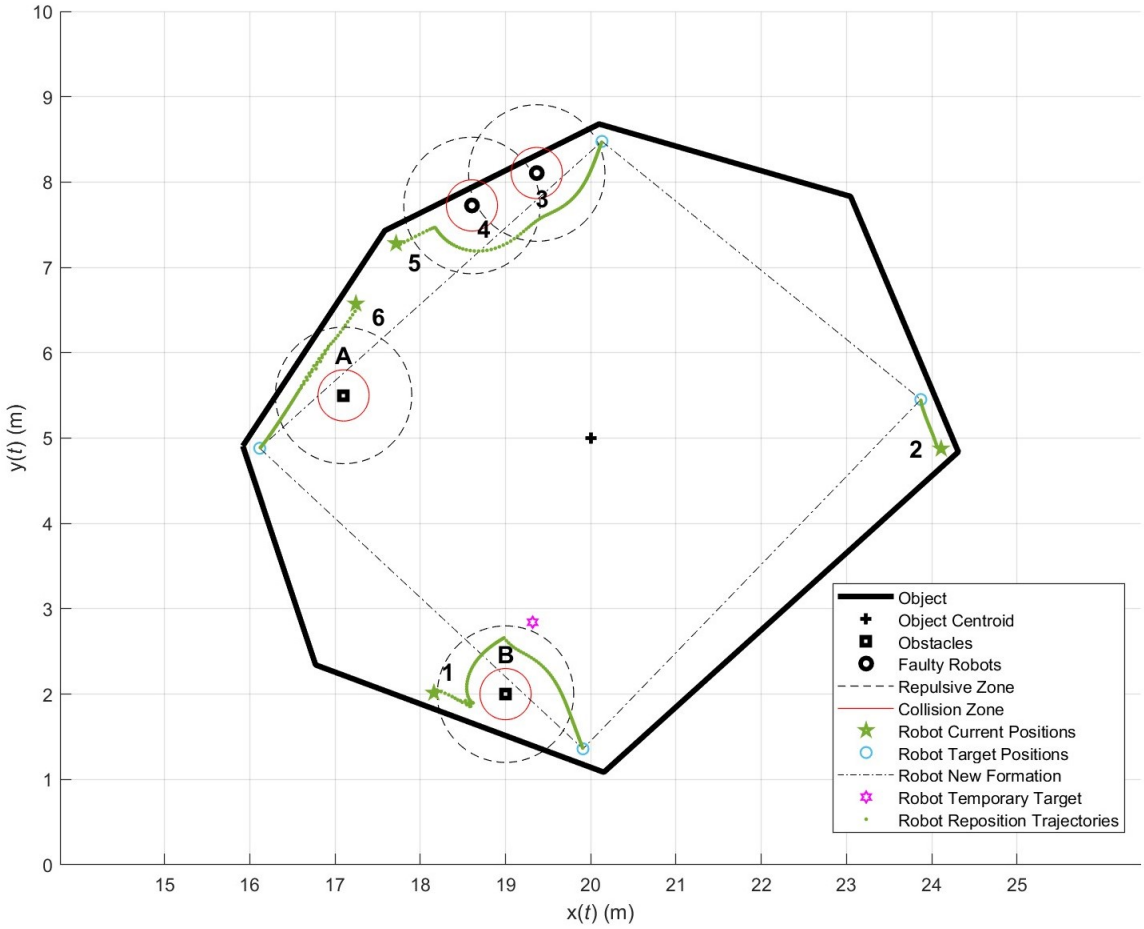

Figure 3.11: Formation reconfiguration for the remaining four healthy robots of an MRS with six robots suffering from severe faults (b)

As shown in Figure 3.11, obstacle A is close to the object boundary and near the path of robot 6. When the robot 6 enters the repulsive field of obstacle A, it moves along inside of the object boundary towards the target. Robot 1 enters the repulsive field of obstacle B, while already in the repulsive field of the object boundary, and it becomes trapped in a local minimum of the IAPF. The robot finds a temporary target to escape the local minimum and reaches its final target successfully. This simulation example illustrates that the proposed IAPF keeps the robots within the object boundaries and permits them to escape local minima.

Simulation Example 3

In Figure 3.12, an object with six vertices is transported by an MRS with four robots, whose robot 2 experiences severe faults during transportation. Hence, new positions are assigned to the remaining three healthy robots. The challenge for the remaining healthy robots in this simulation example is to cooperatively balance the object while they reposition themselves, as discussed in Section 3.6. In the queue, the robot repositioning order is 1–3–4. When evaluating the feasibility of their repositioning, the current and target positions of each robot are on the same side of the line passing through their two neighbors.

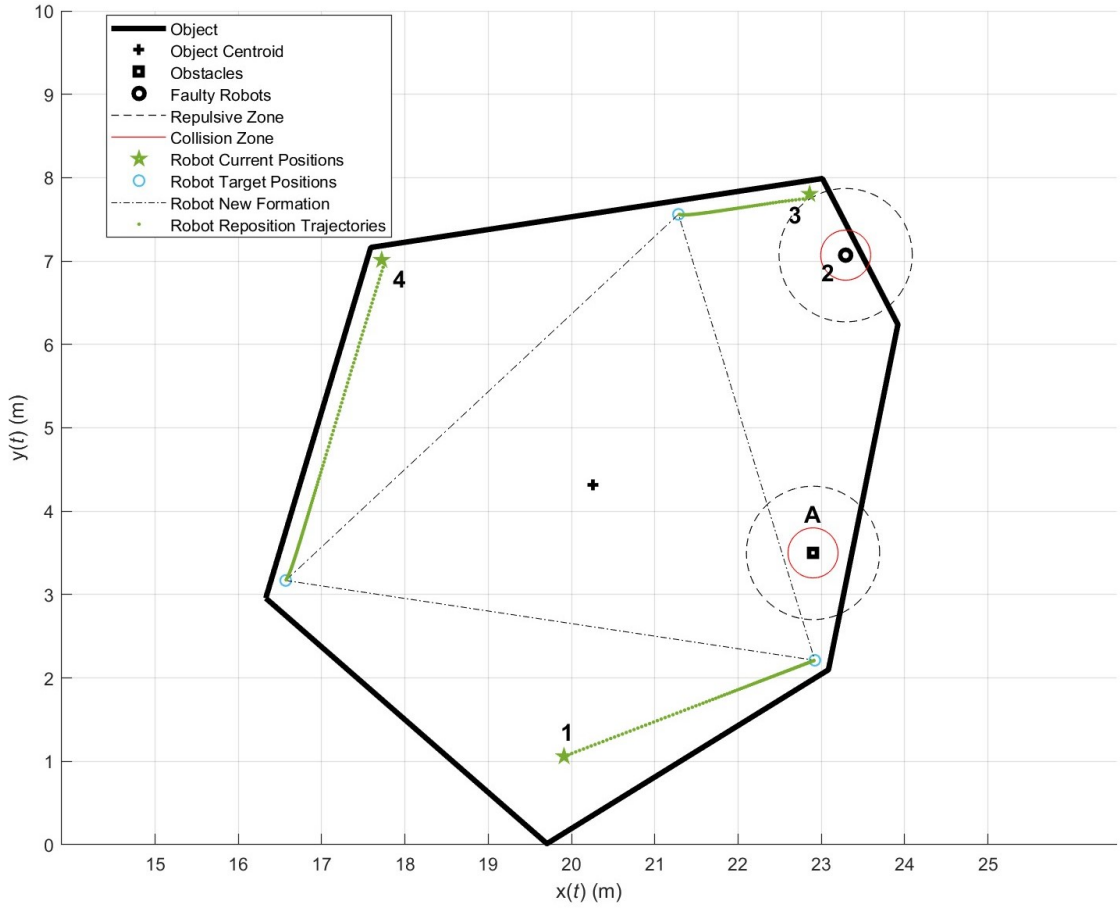

Figure 3.12: Formation reconfiguration for the remaining three healthy robots of an MRS with four robots suffering from severe faults (c)

As shown in Figure 3.12, robot 1 cannot reposition itself under the current formation. The centroid of the object is inside of the triangle formed by the current position of robot 4 with the current and target positions of robot 1. Robot 1 moving to its target position would leave the centroid of the object outside the polygon of the new MRS formation, that is, the new MRS formation would not balance the object. Therefore, robot 1 is not feasible for repositioning at this step. However, after robots 3 and 4 move to their the new positions, robot 1 can reposition itself while balancing the object cooperatively with robots 3 and 4, so the feasible repositioning order for the robots is 3–4–1.

3.8 Summary

This chapter proposes a complete set of strategies for reconfiguring the remaining healthy robots of an MRS when several of its robots severely malfunction while the MRS transports an object by balancing it from below, ensuring the continuous and stable progress of the task after the occurrence of severe faults. The set includes:

1. **Generation of a new optimal formation:** By treating the malfunctioning robots as static obstacles, a constrained optimization function generates the optimal distribution of the healthy robots, to avoid overlapping positions with the malfunctioning robots and ensure the geometric stability of the formation.

2. **Task reassignment:** The Hungarian algorithm assigns new positions to the healthy robots through a cost matrix, to minimize the total moving distance from the current positions of robots to their positions in the new formation, achieving an efficient position assignment.

3. **Path planning and motion control:** An IAPF that superimposes the attractive field of the target with the repulsive fields of the obstacles and of the

object boundary successively guides the healthy robots to their positions in the new MRS formation. By replacing the attractive field of the final target with attractive fields of temporary targets when a robot becomes trapped in a local minimum, the designed IAPF permits all robots to reach their assigned positions in the new formation while avoiding collisions with the malfunctioning robots and environment obstacles, and moving only under the object to continuously contribute to the balance the object.

4. **Cooperative balance strategy:** Half-plane determination and triangular region analysis identify the order in which the remaining healthy robots reposition themselves to cooperatively balance the object at all times.

5. **Simulation verification:** Three simulation scenarios verify the effectiveness of the proposed formation reconfiguration strategies different fault scales, complex environments, and boundary constraints. The results show that the proposed strategies can effectively handle various fault scenarios and efficiently and stably reconfigure the MRS formed by the remaining healthy robots.

Chapter 4

Transportation Task Resumes after Healthy Robots Reposition or in Fault Free Case

Once the MRS formed by the remaining healthy robots reconfigures itself in the new optimal formation, the MRS resumes the object transportation task. Modeling the MRS transportation system is modeled as a coupled rigid-body structure, where each healthy robot is equivalent to a "steering wheel" of the system, all its robots need to move with the same velocity to ensure that the MRS transports the object along the planned path. However, the severely faulty robots are now additional static obstacles in the environment, and the MRS must avoid collisions during the journey. Therefore, this chapter extends the IAPF method to the path planning and motion control of the entire MRS. It builds a resultant potential field for the MRS by superimposing an attractive potential field of the target position of the object and repulsive potential fields for obstacles, to guide the centroid of the object to move along a safe path. Trapping in local minima is avoided through an escape strategy based on

temporary target points. The optimal temporary target is provided by a multi-step optimization that ensures that the MRS can continuously approach the final target in a complex environment. Three simulation examples verify the effectiveness of the method, illustrating different fault scenarios and obstacle configurations.

4.1 Multi-Robot Transportation System Obstacles Avoidance

After the MRS has reconfigured its formation, the object transportation task resumes. The MRS transportation system is modeled as a coupled rigid-body structure, with each robot providing a steering wheel [56]. Namely, the MRS is modeled as a single robot with multiple steering wheels moving the object to its destination through translation, so all robots move with the same velocity. The centroid of the object represents its position. Since the severely malfunctioning robots are now static obstacles, the new MRS needs to avoid collision with them. To this end, the IAPF from Section 3.3 is modified to be applied to the entire MRS.

Let the position of the object be $\mathbf{c}_o = \begin{pmatrix} c_{o_x} & c_{o_y} \end{pmatrix}^\intercal$, and its target position be $\mathbf{c}_d = \begin{pmatrix} c_{d_x} & c_{d_y} \end{pmatrix}^\intercal$. The obstacle position is $\mathbf{q}_{obs.h_i} = \begin{pmatrix} x_{obs} & y_{obs} \end{pmatrix}^\intercal$. The new MRS, comprising the remaining healthy robots, is $\mathbf{r}_{health} = [\mathbf{q}_{h_1}, \mathbf{q}_{h_2}, \cdots, \mathbf{q}_{h_{n-m}}]^\intercal$ with $n - m \geq 3$; each healthy robot has coordinates $\mathbf{q}_{h_i} = \begin{pmatrix} x_{h_i} & y_{h_i} \end{pmatrix}^\intercal$ with $i \in \{1, 2, \cdots, n - m\}$.

The target position of the object contributes the attractive potential component of the IAPF. From Equation (3.6), the attractive force $\mathbf{F}_{att}(\mathbf{c}_o)$ on the object can be computed by:

$$\mathbf{F}_{att}(\mathbf{c}_o) = k_{att} \cdot (\mathbf{c}_d - \mathbf{c}_o) \tag{4.1}$$

where k_{att} is the constant of the attractive potential field.

In addition to moving towards the target position, the MRS needs to prevent collisions between the wheels and the obstacles. The environment obstacles and the faulty robots each provide repulsive potentials. Then, multiple repulsive forces may simultaneously act on multiple robots. The repulsive force on each robot can be obtained by:

$$\begin{aligned}
\mathbf{F}_{rep.h_i}(\mathbf{q}_{h_i}) &= \begin{cases} \mathbf{F}_{rep.o1.h_i}(\mathbf{q}_{h_i}) + \mathbf{F}_{rep.o2.h_i}(\mathbf{q}_{h_i}) & \rho_{rep.o.h_i} \leq \rho_o \\ 0 & \rho_{rep.o.h_i} > \rho_o \end{cases} \\
\mathbf{F}_{rep.o1.h_i}(\mathbf{q}_{h_i}) &= k_{rep.o}\left(\frac{1}{\rho_{rep.o.h_i}} - \frac{1}{\rho_o}\right)\frac{\rho_{att.h_i}^n}{\rho_{rep.o.h_i}^2} \cdot \frac{\mathbf{q}_{h_i} - \mathbf{q}_{obs.h_i}}{\rho_{rep.o.h_i}(\mathbf{q}_{h_i})} \\
\mathbf{F}_{rep.o2.h_i}(\mathbf{q}_{h_i}) &= \frac{n}{2}k_{rep.o}\left(\frac{1}{\rho_{rep.o.h_i}} - \frac{1}{\rho_o}\right)^2 \rho_{att.h_i}^{n-1} \cdot \frac{\mathbf{q}_{h_{d_i}} - \mathbf{q}_{h_i}}{\rho_{att.h_i}(\mathbf{q}_{h_i})}
\end{aligned} \tag{4.2}$$

where $\rho_{rep.o.h_i}(\mathbf{q}_{h_i}) = ||\mathbf{q}_{h_i} - \mathbf{q}_{obs.h_i}||$ is the distance between the robot and the obstacle, and $\rho_{att.h_i}(\mathbf{q}_{h_i}) = ||\mathbf{q}_{h_{d_i}} - \mathbf{q}_{h_i}||$ is the distance between the current position and the desired position of the robot; ρ_o is the range of the repulsive potential field of the obstacle; $k_{rep.o}$ is the constant of the repulsive potential field constant, and n is the IAPF exponent, an positive number.

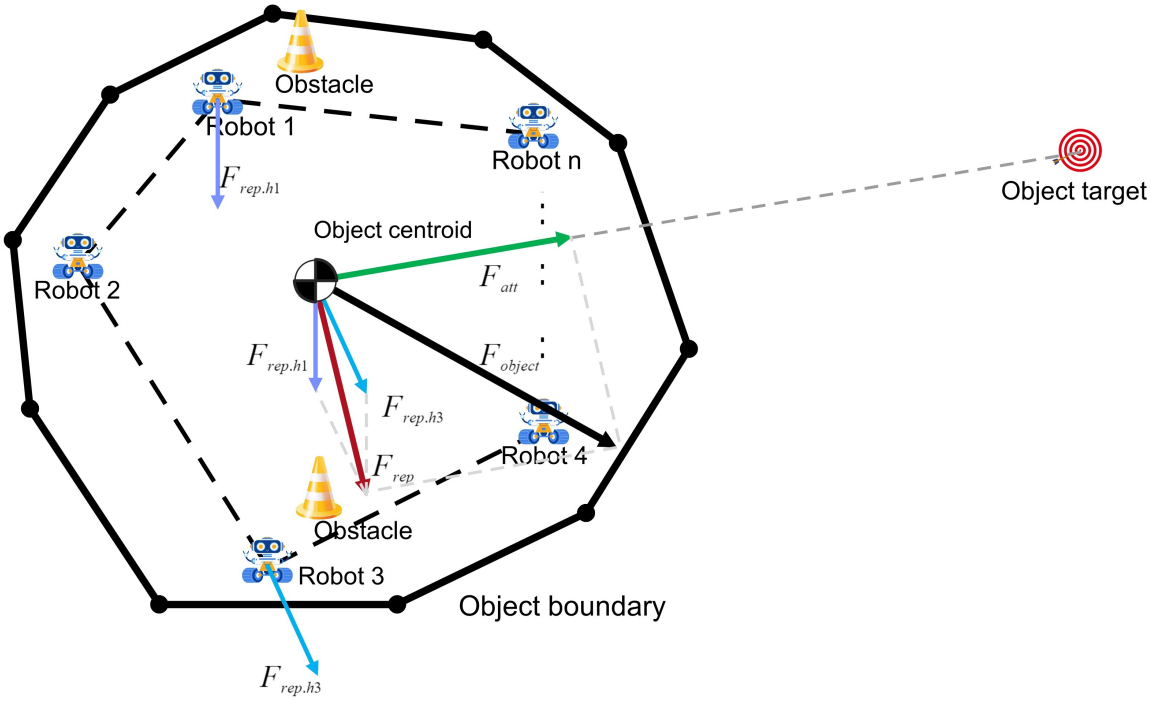

Figure 4.1: Resultant forces on an MRS in an IAPF potential field

As shown in Figure 4.1, the force that guides the MRS to move towards the target position and avoid collisions is the sum of the attractive force and all the repulsive forces at the centroid of the object:

$$\mathbf{F}_{object} = \mathbf{F}_{att}(\mathbf{c}_o) + \sum_{i=1}^{n-m} \mathbf{F}_{rep.h_i}(\mathbf{q}_{h_i}) \tag{4.3}$$

This force provides the velocity command for the MRS as it moves towards the target and avoids collisions with the malfunctioning robots and other environment obstacles.

4.2 Escaping Local Minimum by Temporary Target Point

To avoid the trapping of the MRS at a local minimum in the potential field that results from the superposition of the attractive field of the target with the repulsive fields of the malfunctioning robots and environment obstacles, this section develops a similar, four steps, method to find a temporary target for the entire MRS.

- **Step 1: Locating all involved obstacles**

  Multiple robots may encounter multiple obstacles, so as long as the robot is inside of the repulsive range of the obstacle, the obstacle is considered to be involved.

- **Step 2: Obtaining all temporary target position candidates**

  Similar to the step 2 in Section 3.4, for each robot, from the corresponding involved obstacles, the temporary target points are found by Equation (3.12).

- **Step 3: Locating feasible temporary target position candidates**

  Since all robots move with the same velocity, one temporary target position of one robot can map to all other robots. All the mapped temporary target positions need evaluation, and only the points that locate outside of all other potential fields of involved obstacles are the feasible temporary target point candidates.

- **Step 4: The best temporary target position**

  To enhance the likelihood of escaping a local minimum, the MRS should move in the direction with the largest deviation from its initial direction. To this end, all feasible temporary targets are mapped to the centroid of the object. Then,

the optimal target is selected as the one in the direction with the largest acute angle with the direction to the real target.

4.3 Implementation and Simulation

This section presents three simulated MRSs whose remaining healthy robots resume the transportation of the object after they have accommodated the severe faults. The simulations validate that the IAPF methods from Section 4.1 can guide the MRS to move the object towards the target position while avoiding collisions and escaping local minima. The three simulation examples are linked to the three examples of formation reconfiguration for remaining healthy robots in the Section 3.7, to show different scenarios. Table 4.1 gives the parameters used in the simulations.

	Parameter	Value
v_{max}	- maximum speed of robots	10m/s
k_{att}	- constant of the attractive potential	15
$k_{rep,o}$	- constant of the repulsive potential of the obstacle	1
ρ_o	- range of repulsive potential of the obstacle	0.8m
ρ_c	- obstacle collision range (radius)	0.3m
n	- IAPF exponent [64]	2

Table 4.1: IAPF parameters for MRS transportation

Simulation Example 1

As shown in Figure 4.2, the remaining six healthy robots continues the object transportation task. The six robots with severe faults are static obstacles (depicted as black circles in the figure). The obstacles A, B, C, D, and E are from the environment.

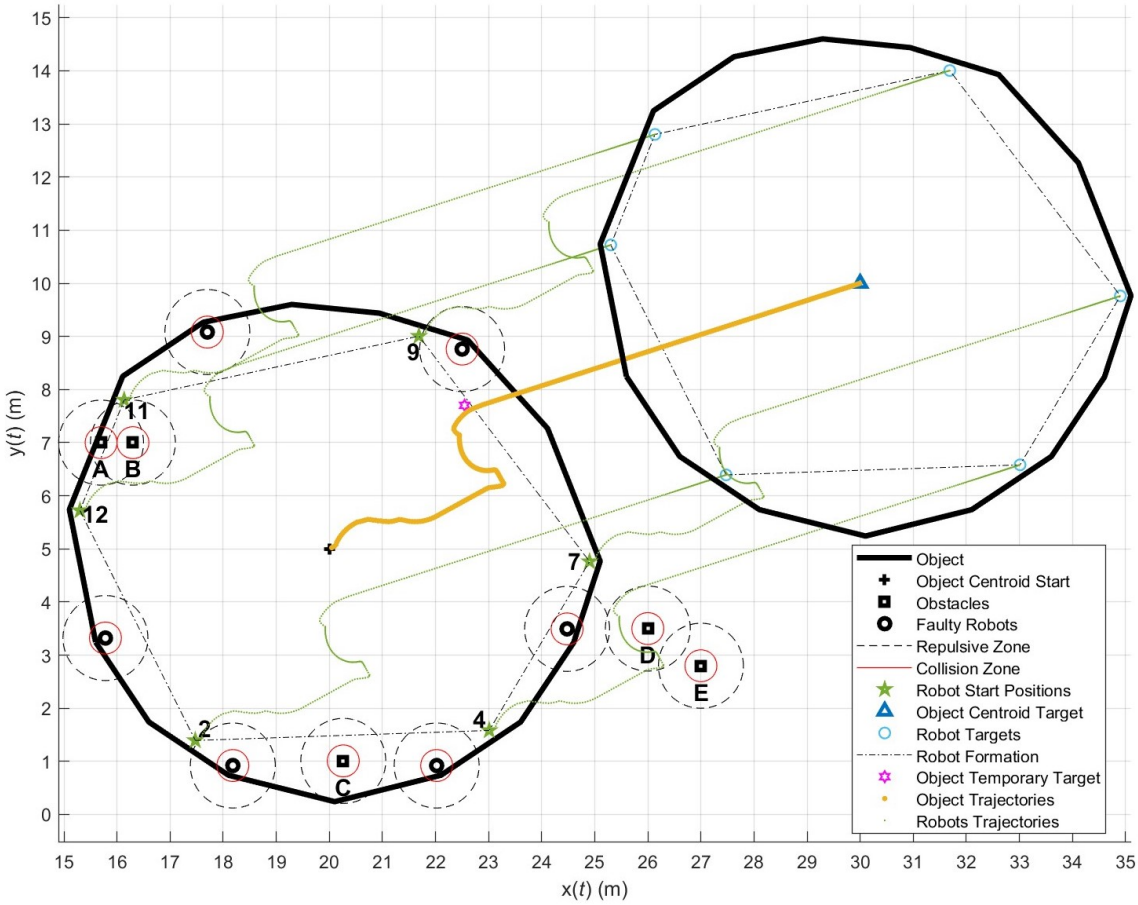

Figure 4.2: Multi-robot transportation mission resumption for the remaining six healthy robots avoid collision from environment obstacles (a)

During the transportation of the object to the target, the curved trajectory initially occurs when robot 9 encounters a malfunctioning robot. Subsequently, robot 12 encounters with obstacles A and B, followed by robot 11 entering the repulsive potential of another malfunctioning robot. When robot 4 enters the overlapping repulsive influence regions of obstacles D and E, the MRS becomes trapped in a local minimum. To resolve this, a temporary target point is selected for the MRS to let it escape. After reaching the temporary target, the MRS moves directly toward the original final target, as a successful mission.

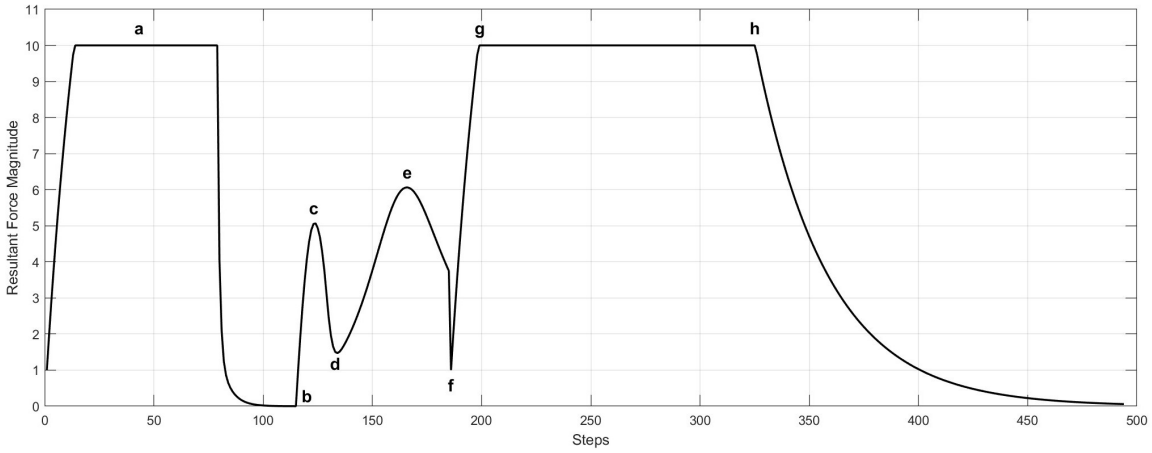

Figure 4.3: The resultant control force on entire MRS

Figure 4.3 shows the resultant force on the MRS. Initially, this force directs the MRS to navigate around obstacles at its maximum speed (10 m/s). At point b, the system becomes trapped in a local minimum when the resultant force drops to zero. Upon switching the final target to a temporary target position, the guidance force increases to point c on the graph. While traveling to the temporary target, robot 4 enters a repulsive field, which causes fluctuations in the resultant forces, as shown in Figure 4.3, from c to f. After escaping the local minimum, the system switches to its original final target, and the control force jumps from point f to point g; the control then decreases gradually as the system approaches the final target.

Simulation Example 2

In the simulation example 2, four remaining healthy robots continue the transportation mission, as shown in the Figure 4.4. The two malfunctioning robots are static obstacles, the black circles in the Figure 4.4. A and B are environment obstacles. During the journey toward the target, robot 1 and robot 5 encounter obstacles A and B, respectively, simultaneously. Obstacle B pushes robot 1 upwards, but obstacle

A pushes robot 5 downwards, trapping the MRS into a local minimum. Then, the escape from a local minimum process is triggered by heading to a temporary target. Different from the simulation example 1, the local minimum is caused by two repulsive forces in different directions acting on the two robots. The temporary target point successfully lets the MRS escape the local minimum.

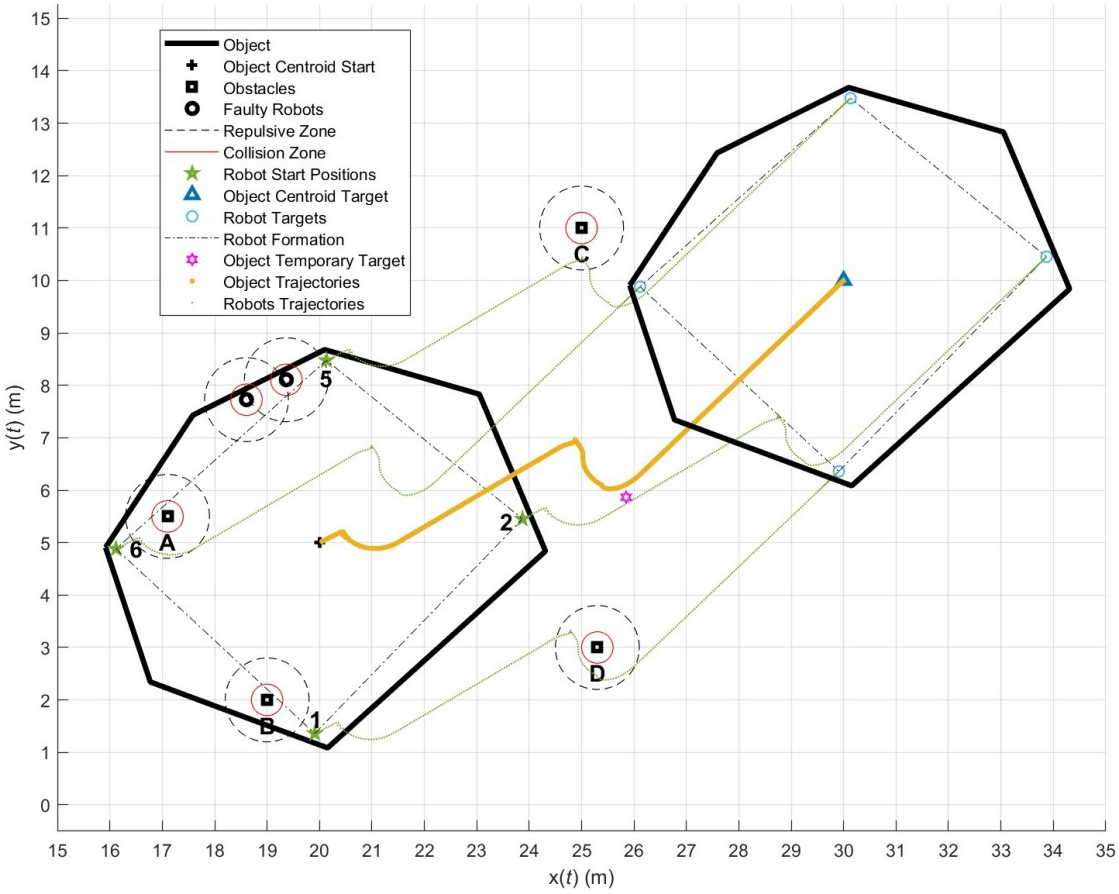

Figure 4.4: Multi-robot transportation mission resumption Multi-robot transportation mission resumption for the remaining four healthy robots avoid collision from environment obstacles (b)

Simulation Example 3

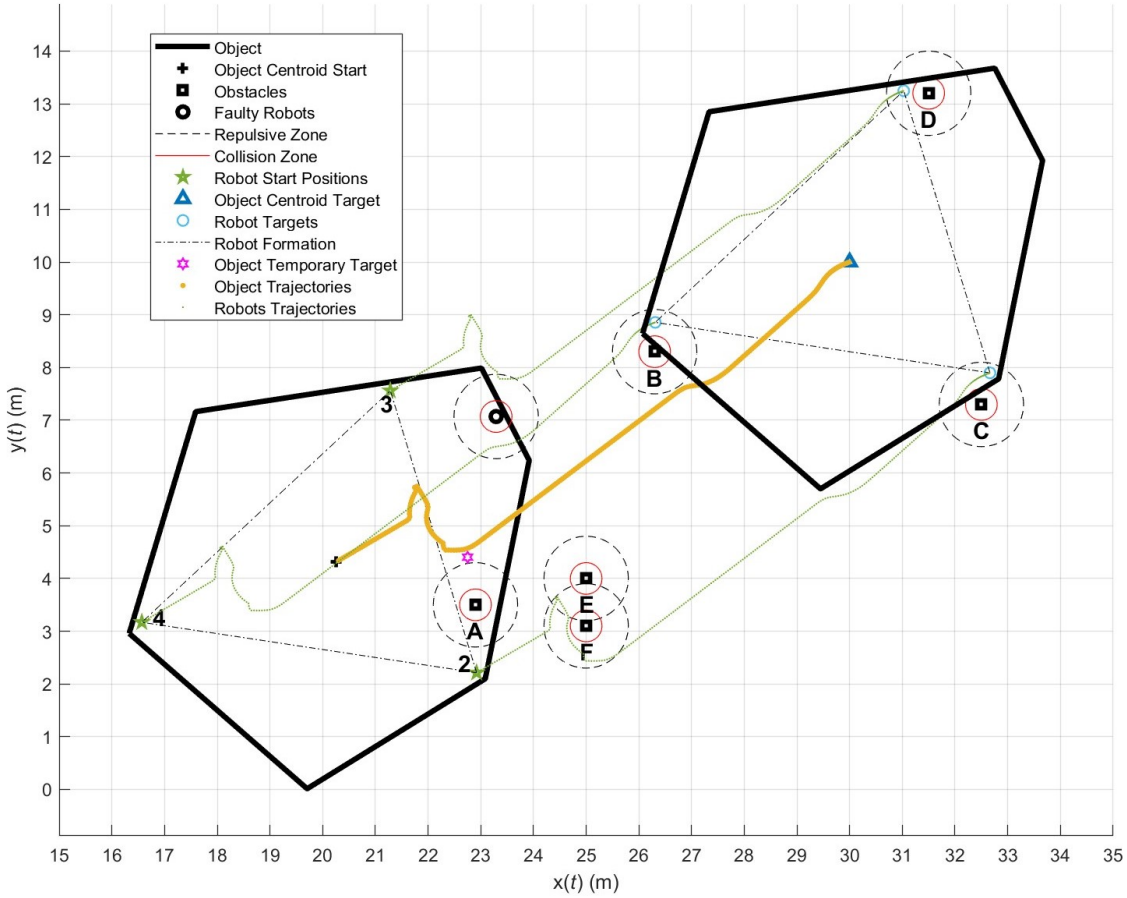

Figure 4.5: Multi-robot transportation mission resumption Multi-robot transportation mission resumption for the remaining three healthy robots avoid collision from environment obstacles (c)

In Figure 4.5, three remaining healthy robots continue the transportation mission, and it is the minimum number of robots required to balance the object. The one malfunctioning robot is a static obstacle, the black circle in the figure. A, B, C, D, E and F are the environment obstacles. This example provides another illustration of the robustness of the proposed IAPF algorithm. Namely, it shows that the IAPF lets an MRS to successfully resume the transportation after severe faults accommodation provided minimum three robots remain healthy.

4.4 Summary

This chapter presents a IAPF-based cooperative transportation resumption control strategy after healthy robots reposition or for fault-free transportation. The strategy effectively addresses the challenges of obstacle avoidance and local minima. The MRS transporting the object is modeled as a coupled rigid-body structure. The centroid of the object is a reference point, and a resultant control force guides the system along a safe path. A four-step optimization process determines the temporary target point. By identifying related obstacles, generating candidate temporary targets, screening feasible solutions, and optimizing the direction deviation, the MRS can escape local minima where the resultant force is zero, to continue its movement towards the final target. Three simulations with various numbers of healthy robots verify the effectiveness of the proposed path planning and control method. The results show that the remaining MRS can successfully avoid static obstacles and faulty robots and escape local minima.

Chapter 5

Multi-Robot Transportation System with Severe Faults Accommodation: Implementation and Results

This chapter validates the proposed framework for handling severe faults in MRS transportation systems through Matlab simulations, demonstrating the complete process from initial formation generation to post-fault task resumption. The MRS transportation task is to move an object, modeled as a 2-D convex polygon, from an initial to a final position after distributing its robots under the object to stably support it from below during transport. The MRS must move the object from starting point "I" to endpoint "III", and six robots experience severe faults at point "II" to verify ability of the remaining healthy robots to resume the transportation after they reconfigure themselves into a new formation to continue to optimally balance the object during transport.

5.1 Implementation and Simulation

The simulation example in this chapter presents a complete transportation mission by an MRS equipped with the path planning and control algorithms proposed in the previous chapters for severe faults accommodation, including the initialization of the optimal robot formation, the transportation in fault-free case,the reconfiguration of the remaining healthy robots in a new optimal formation when faults occur and the resumption of the transportation mission. Figure 5.1 shows the object, whose shape is randomly generated. The object is assumed to be rigid, with uniform thickness and density, with convex polygonal top and bottom surfaces, so it can be simplified as a 2-D convex polygon, whose location is its center of gravity. The robots lift and support the object from underneath and translate it during transportation. The parameters selected for this simulation are shown in Table 5.1.

A ten-robots MRS is assigned to transport the object from the location "I" to location "III" and pass through location "II". At the location "II", six robots experience severe faults, and are not able to continue the object transportation task. During transportation, the centroid of the object represents its location, as well as the location of the MRS. On the path to the final target, the MRS needs to avoid collisions with the environmental obstacles A, B, C, D, E, F, G, H, I. Lastly, the severely faulty robots become additional obstacles at location "II".

	Parameter	Value
r	- radius of robots	0.1m
v_{max}	- maximum speed of robots	10m/s
d_r	- minimum distance between robots	0.6m
ω	- weight factor	0.5
k_{att}	- constant of the attractive potential	6
$k_{rep,o}$	- constant of the repulsive potential of the obstacle	1
ρ_o	- range of repulsive potential of the obstacle	0.8m
ρ_c	- obstacle collision range (radius)	0.3m
$k_{rep,e}$	- constant of the potential foeld of the object edges	0.5
ρ_e	- range of the repulsive potential of the object edges	0.2m
n	- IAPF exponent [64]	2

Table 5.1: Parameters for initial optimal MRS formation, healthy robot formation reconfiguration and MRS transportation by IAPF

Initially, at the starting location of the transportation mission, the SQP solution of the optimization proposed in Equation (2.12) initializes the formation of the ten robots such that each robot and the boundaries of the MRS formation are as far as possible from the centroid of the object, as shown in the detailed plot at the right upper corner in Figure 5.1. Next, the IAPF algorithm proposed in Section 4.1 guides the 10-robot MRS to avoid collisions with environment obstacles. As show in Figure 5.1 from location "I" to location "II", the system encounters four obstacles A, B, C and D. First, robot 5 meets obstacle A and moves around it to cause the first curved part of the path of the MRS. Then, when both robots 5 and 6 encounter obstacle C, the resultant control force approaches zero, and the MRS becomes trapped in the local minimum. The proposed four-step method from Section 4.2 identifies an optimal temporary target. The attractive potential temporarily switches to the

temporary target, dragging the MRS out of the local minimum successfully. After the MRS is nearby the temporary target, the proposed algorithm deactivates it and reactivates the original final target such that the MRS moves towards it again.

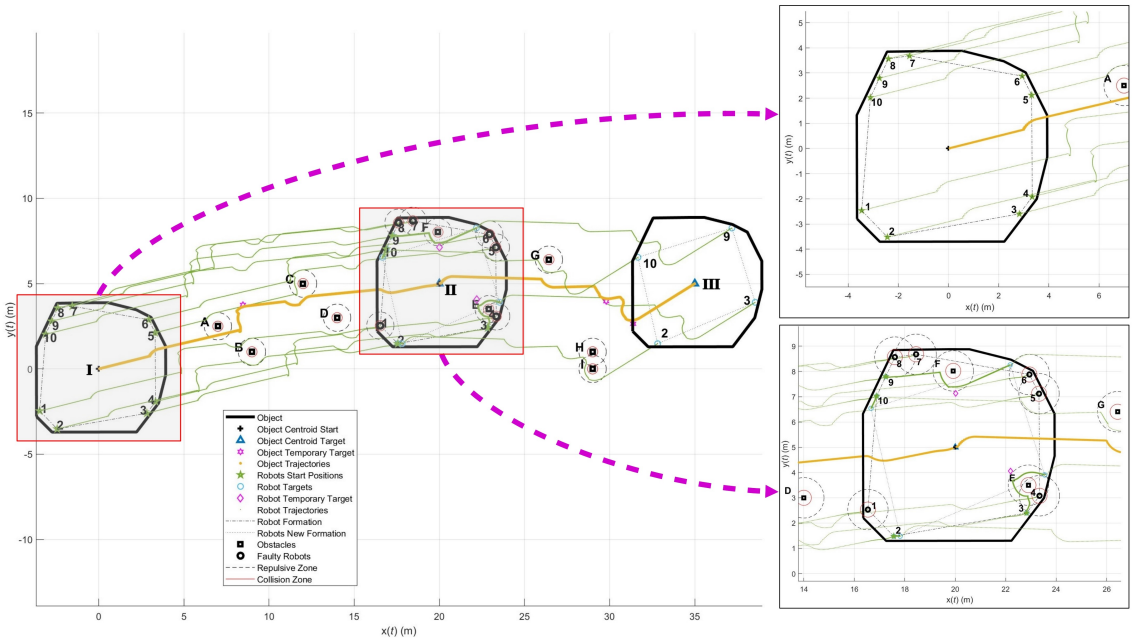

Figure 5.1: Initial optimal formation of a 10 robots MRS transporting a convex object with six robots suffering from severe faults and remaining four healthy robots continuing the mission

At location "II", as illustrated in the detailed figure at the lower right corner in Figure 5.1, six robots experience severe faults, and are subsequently treated as obstacles and indicated by black circles. The transportation pauses for faults accommodation. The SQP solution of the optimization (Equation (3.2)) generates a new formation for the remaining healthy robots to continue the transportation task. Then, the Hungarian algorithm in Section 3.2 assigns each healthy robot to a unique position in the new formation. Next, the IAPF in Section 3.3 guides the robots for formation reconfiguration. Robots 2 and 10 move directly to their new positions, as there are no obstacles on their paths. Obstacle F is in the path of robot 9, right in front of the robot. The robot gets trapped in the local minimum when it enters the repulsive

field of obstacle F, which is the scenario introduced in Figure 3.2 from Section 3.4. To escape from the local minimum area, the four-steps planning strategy proposed in Section 3.4 identifies a temporary target point, and the robot escapes the local minimum by heading towards the temporary target; then, it continues to travel towards its assigned position in the new MRS formation. Robot 3 falls into a local minimum when it encounters obstacle E and the faulty robot 4. The overlapped repulsive fields lead to zero resultant force on the robot, which is another scenario introduced in Figure 3.3 from Section 3.4. A temporary target point helps the robot escape the local minimum, and to reach its assigned position in the new MRS formation. During the entire formation reconfiguration, the robots cooperatively balance the object all the time. Although not obvious in this simulation example, the cooperative path planning strategies introduced in Section 3.6 apply. The initial robot repositioning order requires no changes in this example. Once all remaining healthy robots reach their reassigned positions, they resume the object transportation mission.

Moving from location "II" to "III", the MRS comprising the remaining four healthy robots needs to avoid collisions with the faulty robots and with the environment obstacles G, H and I. As in the fault-free case, as shown in Figure 5.1, the four-robot MRS successfully passes around the faulty robots. However, it gets trapped in local minima twice when robot 5 encounters with obstacle G and when robot 2 encounters obstacles H and I. The temporary target positions guide the MRS to escape the local minima and to successfully transport the object to its final position.

5.2 IAPF Resultant Force Analysis

Robot 3

At the location II where the four healthy robots reposition themselves the mag-

nitude of the resultant force on robot 3 during repositioning is shown in Figure 5.2.

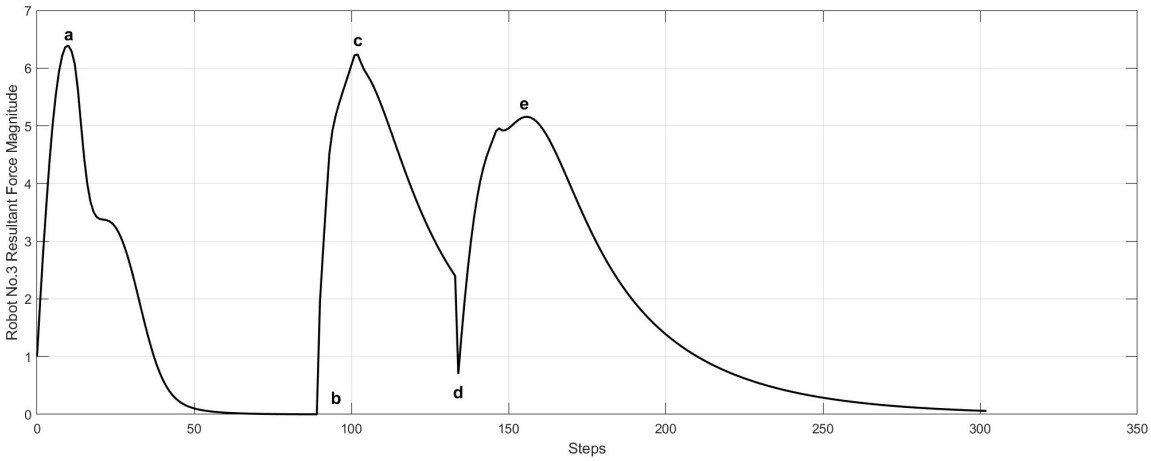

Figure 5.2: The resultant control force of robot 3 during repositioning

Initially, before the robot encounters any obstacles or malfunctioning robots, the robotis only attracted by its new position and moves directly towards it. However, obstacle F is right on its path and traps it into a local minimum. The resultant force on robot 3 drops from a to zero at b, as shown in Figure 5.2. The temporary target point leads to an increase in the magnitude of the resultant force to c, and the robot escapes the local minimum. Then, when the robot approaches the temporary target, the resultant force decreases to d. After escaping the local minimum, the robot switches back to its original final target position, and the magnitude of the resultant force on it increases to e, guiding the robot to its desired position.

Robot 9

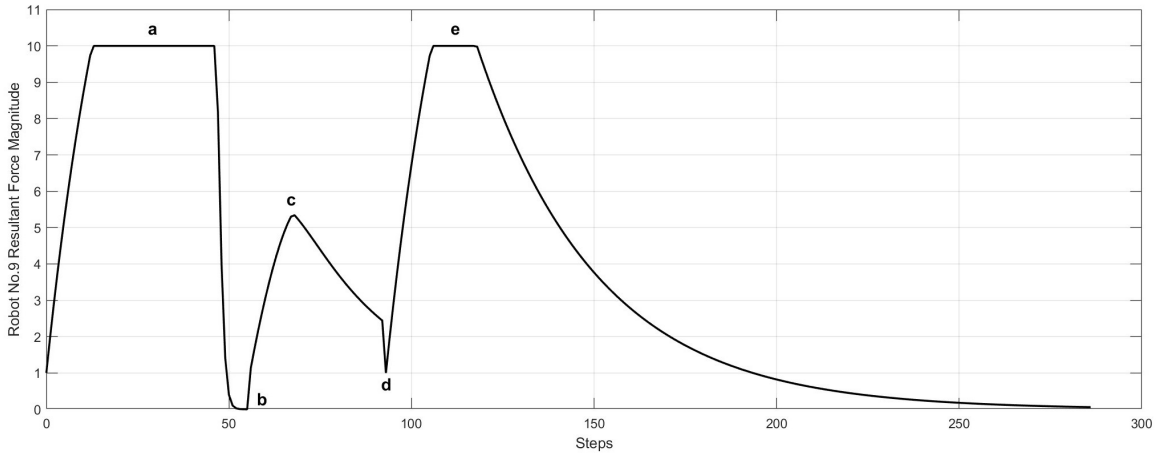

Figure 5.3: The resultant control force of robot 9 during repositioning

As shown in Figure 5.3, when robot 9 encounters obstacle E and the malfunctioning robot 4, as an obstacle, robot 9 is in their overlapped repulsive fields. The resultant force on robot 9 drops from a to b, as the repulsive forces cancel out the attractive force from the final target position, and the robot is trapped in a local minimum when the force drops to zero. The temporary target position increases the resultant force from zero to c, guiding the robot out of the local minimum, and the resultant force drops to d when robot 9 approaches the temporary target.

MRS Transportation System

At location II, after the repositioning of the remaining healthy robots, the MRS resumes the object transportation. The resultant force acting on the MRS as it travels from location II to location III is shown in the Figure 5.4.

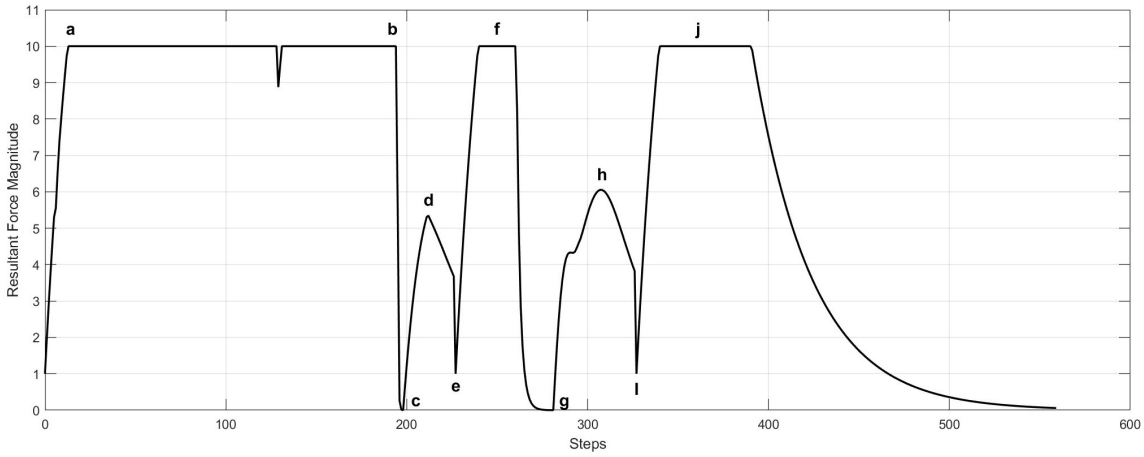

Figure 5.4: Resultant force on the four-robot MRS as it transports the object from location II to location III

From a to b in Figure 5.4, there is a drop of the magnitude of the resultant force, as robot 10 encounters the malfunction robot 5. Moving forward, the obstacle G is right in front of robot 10. As a result, the resultant force drops to zero at c, so the MRS falls into a local minimum. After the selection of an optimal temporary target, its attractive field breaks the balance of control forces (local minimum), and the resultant force increases from c to d, dragging the MRS out of the local minimum. The force drops when the MRS gets closer to the local minimum and increases to f when the final target becomes attractive again. Lastly, the resultant force drops to zero at g (local minima) when robot 2 encounters obstacles H and I, falling into overlapping repulsive fields. One last time, the temporary target strategy helps the MRS escape the local minium.

5.3 Summary

This chapter validates the complete implementation of the framework for handling severe faults in MRS transportation systems through a Matlab simulation of a ten-

robot MRS tasks to move a 2-D convex polygonal object from a starting point "I" to a target point "III". At point "II", six robots experience severe faults, and the remaining healthy robots must navigate environmental obstacles and faulty robots. The framework generates initial and post-fault MRS formations through optimizing the stability of the object balance, completes task reassignment via the Hungarian algorithm, and plans obstacle-free paths combining the IAPF method with a temporary target point strategy to escape local minima. Simulation results verify the feasibility and effectiveness of the proposed framework.

Chapter 6

Conclusion and Future Work

6.1 Conclusion

This thesis tackles the handling of severe faults in multi-robot transportation systems. MRS have significant advantages over single-robot systems in terms of collaborative intelligence, task expandability, and system reliability. However, dealing with severe faults such as motor burnout or structural damage still remains challenging in generating new formations for healthy robots, reallocating tasks and planning paths during reconfiguration, and safely resuming transportation tasks. To address these challenges, a severe fault accommodation framework is proposed, based on optimal formation generation and the IAPF method, forming a complete solution through theoretical modeling, algorithm design, and simulation validation.

The thesis formulates the optimal position distribution of robots as a constrained optimization problem to maximize the stability of the MRS balancing the object for transportation. The objective function maximizes the distance from the centroid of the object to the robots and to the boundaries of the MRS formation, and the constraints include distribution range, collision avoidance, and inclusion of the centroid

of the object. When faults occur, faulty robots become obstacles, and the proposed MRS formation optimization framework generates the new formation for the remaining healthy robots. The Hungarian algorithm assigns a position to each healthy robot in the new formation, to minimize the total movement distance and reduce energy consumption during reconfiguration. The IAPF method, with attractive forces, obstacle repulsion, and boundary repulsion, guides the MRS to the target, incorporating a temporary target point strategy to escape local minima. A cooperative strategy based on half-plane determination and triangular region analysis ensures the object balance during reconfiguration by verifying that the MRS formation includes the centroid of the object at all times. The transportation system is treated as a rigid body, containing the robots and the object, and the IAPF guides the centroid of the object to move as one piece such that all robots avoid obstacles at all times.

Simulations validate the framework on initial formation generation for objects with various convex polygonal shapes, for MRSs with various numbers of robots, formation reconfiguration when severe faults occur, and task resumption with obstacle avoidance. The results illustrate the effectiveness and robustness of the framework.

6.2 Future Work

Future work can focus on reconfiguration to accommodate severe faults without mission suspension. The current framework requires pausing the transportation upon detecting severe faults to complete formation reconfiguration. However, real-world applications such as emergency material transportation and high-risk environment operations may demand continuous task execution. Thus, breaking through the process of "pause-reconfigure-resume" to achieve real-time reconfiguration in dynamic environments is an important next step.

Also, a coupled model considering the robot and object dynamics can be developed to support reconfiguration during task execution. This research simplifies the system by considering force controlled robots. In the future, a multi-body dynamic model can characterize the dynamic interaction between robot driving forces, frictional forces, and object inertial forces. Dynamic stability indicators can be introduced into the formation and reconfiguration objective function, and the acceleration trajectories of the healthy robots can be optimized during repositioning, enabling the robots to dynamically maximize the stability of the object transportation. Moreover, a force-feedback based cooperative control strategy can be designed to detect a robot failure, and adjacent robots can sense load changes through force sensors and actively adjust driving speed to maintain object balance, while other healthy robots gradually move to new positions along dynamically feasible paths to form a transitional formation, avoiding mission suspension.

Additionally, this thesis considers only holonomic robots. Non-holonomic robots can be considered (e.g., differential-drive wheeled robots, UAV) by embedding constraints on the minimum turning radius into the reconfiguration algorithm, to both ensure object balance conditions and robot reachability.

For increased practicality, 3-dimensional MRS transportation, whereby the robots move on uneven terrain, and dynamic obstacles should also be considered.

Bibliography

[1] P. U. Lima and L. M. Custódio, *Multi-Robot Systems*. Berlin, Heidelberg: Springer Berlin Heidelberg, 2005, pp. 1–64.

[2] b. Zhou, R. Zhou, Y. Gan, F. Fang, and Y. Mao, "Multi-robot multi-station cooperative spot welding task allocation based on stepwise optimization: An industrial case study," *Robotics and Computer-Integrated Manufacturing*, vol. 73, 2022.

[3] A. Dutta, S. Roy, O. P. Kreidl, and L. Bölöni, "Multi-robot information gathering for precision agriculture: Current state, scope, and challenges," *IEEE Access*, vol. 9, pp. 161 416–161 430, 2021.

[4] S. DiMaio, M. Hanuschik, and U. Kreaden, *The da Vinci Surgical System*. Boston, MA: Springer US, 2011, pp. 199–217. [Online]. Available: https://doi.org/10.1007/978-1-4419-1126-1_9

[5] M. A. Kamel, X. Yu, and Y. Zhang, "Real-time fault-tolerant formation control of multiple wmrs based on hybrid ga–pso algorithm," *IEEE Transactions on Automation Science and Engineering*, vol. 18, no. 3, pp. 1263–1276, 2021.

[6] X. An, C. Wu, Y. Lin, M. Lin, T. Yoshinaga, and Y. Ji, "Multi-robot systems and cooperative object transport: Communications, platforms, and challenges," *IEEE Open Journal of the Computer Society*, vol. 4, pp. 23–36, 2023.

[7] Z. Yan, N. Jouandeau, and A. Ali-Chérif, "Multi-robot heuristic goods transportation," in *2012 6th IEEE International Conference Intelligent Systems*. IEEE, 2012, pp. 409–414.

[8] D. Koung, O. Kermorgant, I. Fantoni, and L. Belouaer, "Cooperative multi-robot object transportation system based on hierarchical quadratic programming," *IEEE Robotics and Automation Letters*, vol. 6, no. 4, pp. 6466–6472, 2021.

[9] R. Tinós, M. H. Terra, and M. Bergerman, "A fault tolerance framework for cooperative robotic manipulators," *Control Engineering Practice*, vol. 15, no. 5, pp. 615–625, 2007.

[10] Q. Xu, H. Yang, B. Jiang, D. Zhou, and Y. Zhang, "Fault tolerant formations control of uavs subject to permanent and intermittent faults," *Journal of Intelligent and Robotic Systems*, vol. 73, pp. 589–602, 2014.

[11] Y. Wang, Y. Song, and F. L. Song, "Robust adaptive fault-tolerant control of multiagent systems with uncertain nonidentical dynamics and undetectable actuation failures," *IEEE Transactions on Industrial Electronics*, vol. 62, no. 6, pp. 3978–3988, 2015.

[12] M. Saska, T. Krajník, V. Vonásek, Z. Kasl, V. Spurný, and L. Přeučil, "Fault-tolerant formation driving mechanism designed for heterogeneous mavs-ugvs groups," *Journal of Intelligent and Robotic Systems*, vol. 73, pp. 603–622, 2014.

[13] Y. Hua, X. Dong, Q. Li, and Z. Ren, "Distributed fault-tolerant time-varying formation control for second-order multi-agent systems with actuator failures and directed topologies," *IEEE Transactions on Circuits and Systems-II: Express Briefs*, vol. 65, no. 6, pp. 774–778, 2018.

[14] M. Khalili, X. Zhang, Y. Cao, M. M. Polycarpou, and T. Parisini, "Distributed fault-tolerant control of multiagent systems: An adaptive learning approach," *IEEE Transactions on Neural Networks and Learning Systems*, vol. 31, no. 2, pp. 420–432, 2020.

[15] M. Ozkan, G. Kirlik, O. Parlaktuna, A. Yufka, and A. Yazici, "A multi-robot control architecture for fault-tolerant sensor-based coverage," *International Journal of Advanced Robotic Systems*, vol. 7, no. 1, pp. 67–74, 2010.

[16] M. T. Khan, M. U. Qadir, F. Nasir, and C. W. de Silva, "A framework for a fault tolerant multi-robot system," *The 10th International Conference on Computer Science and Education (ICCSE 2015)*, pp. 197–201, 2015.

[17] G. Chen and Y.-D. Song, "Robust fault-tolerant cooperative control of multiagent systems: A constructive design method," *Journal of the Franklin Institute*, vol. 352, pp. 4045–4066, 2015.

[18] H. Yang, B. Jiang, H. Yang, and K. Zhang, "Cooperative control reconfiguration in multiple quadrotor systems with actuator faults," *IFAC-PapersOnLine*, vol. 48, no. 21, pp. 386–391, 2015.

[19] X. Yu, Z. Liu, and Y. Zhang, "Fault-tolerant formation control of multiple uavs in the presence of actuator faults," *International Journal of Robust and Nonlinear Control*, vol. 26, no. 15, pp. 2668–2685, 2016.

[20] H. Yang, Q.-L. Han, X. Ge, L. Ding, Y. Xu, B. Jiang, and D. Zhou, "Fault-tolerant cooperative control of multiagent systems: A survey of trends and methodologies," *IEEE Transactions on Industrial Informatics*, vol. 16, no. 1, pp. 4–17, 2020.

[21] L. Cheng and Y. Wang, "Fault tolerance for communication-based multirobot formation," *Proceedings of the Third International Conference on Machine Learning and Cybernetics*, pp. 172–132, 2003.

[22] R. K. Ramachandran, P. Pierpaoli, M. Egerstedt, and G. S. Sukhatme, "Resilient monitoring in heterogeneous multi-robot systems through network reconfiguration," *IEEE Transactions on Robotics*, vol. 38, no. 1, pp. 126–137, 2022.

[23] O. Khatib, K. Yokoi, K. Chang, D. Ruspini, R. Holmberg, and A. Casal, "Coordination and decentralized cooperation of multiple mobile manipulators," *Journal of Robotic Systems*, vol. 13, no. 11, pp. 755–764, 1996.

[24] A. Marino, "Distributed adaptive control of networked cooperative mobile manipulators," *IEEE Transactions on Control Systems Technology*, vol. 26, no. 5, pp. 1646–1660, 2018.

[25] P. Xu, J. Zhang, Y. Cui, K. Zhang, and Q. Tang, "Modeling and coordinated control of multiple mobile manipulators with closed-chain constraints," *International Journal of Control, Automation, and Systems*, vol. 21, no. 4, pp. 1296–1308, 2023.

[26] Z. Gong, Z. Nie, Q. Liu, and X.-J. Liu, "Design and control of a multi-mobile-robot cooperative transport system based on a novel six degree-of-freedom connector," *ISA Transactions*, vol. 139, pp. 606–620, 2023.

[27] K. Kosuge and T. Oosumi, "Decentralized control of multiple robots handling an object," *Proceedings of the 1996 IEEE/RSJ International Conference on Intelligent Robots and Systems (IROS 96)*, pp. 318–323, 1996.

[28] A. Yufka and M. Ozkan, "Formation-based control scheme for cooperative transportation by multiple mobile robots," *International Journal of Advanced Robotic Systems*, vol. 12, no. 120, pp. 1–19, 2015.

[29] K. Kosuge and M. Sato, "Transportation of a single object by multiple decentralized-controlled nonholonomic mobile robots," *Proceedings of the 1999 IEEE/RSJ International Conference on Intelligent Robots and Systems*, pp. 1681–1686, 1999.

[30] Q. Liu, Z. Quan, Z. Gong, and X.-J. Liu, "An omnidirectional transportation system with high terrain adaptability and flexible configurations using multiple nonholonomic mobile robots," *IEEE Robotics and Automation Letters*, vol. 8, no. 9, pp. 6060–6067, 2023.

[31] Y. Hirata, K. Kosuge, H. Asama, H. Kaetsu, and K. Kawabata, "Coordinated transportation of a single object by multiple mobile robots without position information of each robot," *Proceedings of the 2000 IEEE/RSJ International Conference on Intelligent Robots and Systems*, pp. 2024–2029, 2000.

[32] D. J. Stilwell and J. S. Bay, "Toward the development of a material transport system using swarms of ant-like robots," *Proceedings of the 1993 IEEE International Conference on Robotics and Automation*, pp. 766–771, 1993.

[33] D. P. Bertsekas, "A new algorithm for the assignment problem," *Mathematical Programming*, vol. 21, pp. 152–171, 1981.

[34] T. Li, Y. Li, and Y. Qian, "Improved hungarian algorithm for assignment problems of serial-parallel systems," *Journal of Systems Engineering and Electronics*, vol. 27, no. 4, pp. 858–870, 2016.

[35] C. H. Papadimitriou and K. Steiglitz, *Combinatorial optimization: algorithms and complexity*. Englewood Cliffs, N.J: Prentice Hall, 1982.

[36] P. R. Amal, K. S. Anjumol, S. Unnikrishnan, V. Dilip, and O. George, "Optimized selective assembly using hungarian algorithm," *International Journal of Innovative Science and Research Technology*, vol. 9, no. 8, pp. 1272–1278, 2024.

[37] T. B. Tran and H. H. P. Nguyen, "Optimizing labor allocation based on multiobjective decision making using improved hungarian algorithm," *Journal of Economic Statistics*, vol. 1, no. 3, pp. 16–30, 2023.

[38] L. C. Polymenakos and D. P. Bertsekas, "Parallel shortest path auction algorithms," *Parallel Computing*, vol. 20, pp. 1221–1247, 1994.

[39] K. Clinch, T. A. Wood, and C. Manzie, "Auction algorithm sensitivity for multirobot task allocation," *Automatica*, vol. 158, pp. 1–10, 2023.

[40] J. Erickson, *Algorithms*, 1st ed. University of Illinois at Urbana-Champaign, 2019, pp. 159–186.

[41] L. E. Kavraki, P. Svestka, J.-C. Latombe, and M. H. Overmars, "Probabilistic roadmaps for path planning in high-dimensional configuration spaces," *IEEE Transactions on Robotics and Automation*, vol. 12, no. 4, pp. 56–580, 1996.

[42] S. M. LaValle and J. J. Kuffner, "Randomized kinodynamic planning," *The International Journal of Robotics esearch*, vol. 20, no. 5, pp. 378–400, 2001.

[43] X. Zhang, A. Liniger, and F. Borrelli, "Optimization-based collision avoidance," *IEEE Transactions on Control Systems Technology*, vol. 29, no. 3, pp. 972–982, 2021.

[44] T. Faulwasser and R. Findeisen, "Nonlinear model predictive control for constrained output path following," *IEEE Transactions on Automatic Control*, vol. 61, no. 4, pp. 1026–1035, 2016.

[45] C. W. Warren, "Global path planning using artificial potential fields," *1989 International Conference on Robotics and Automation*, pp. 316–321, 1989.

[46] Y. K. Hwang and N. Ahuja, "A potential field approach to path planning," *IEEE Transactions on Robotics and Automation*, vol. 8, no. 1, pp. 23–32, 1992.

[47] Iswanto, A. Ma'arif, O. Wahyunggoro, and A. I. Cahyadi, "Artificial potential field algorithm implementation for quadrotor path planning," *International Journal of Advanced Computer Science and Applications (IJACSA)*, vol. 10, no. 8, pp. 575–585, 2019.

[48] Y. Zhou, W. Daamen, T. Vellinga, and S. Hoogendoorn, "Review of maritime traffic models from vessel behavior modeling perspective," *Transportation Research Part C: Emerging Technologies*, vol. 105, pp. 323–345, 2019.

[49] Á. Madridano, A. Al-Kaff, D. Martín, and A. de la Escalera, "Trajectory planning for multi-robot systems: Methods and applications," *Expert Systems with Applications*, vol. 173, 2021.

[50] P. adakkepat, K. C. Tan, and M.-L. Wang, "Evolutionary artificial potential fields and their application in real time robot path planning," *The International Journal of Robotics Research*, pp. 256–263, 2000.

[51] H. Wang, L. Wang, X. Gao, X. Yu, C. Lu, and X. Wang, "Uav path planning based on improved artificial potential field method," *Proceedings of 2022 International Conference on Autonomous Unmanned Systems (ICAUS 2022)*, pp. 2930–2939, 2023.

[52] H. Hu, C. Zhang, Y. Sheng, B. Zhou, and F. Gao, "An improved artificial potential field model considering vehicle velocity for autonomous driving," *IFAC PapersOnLine*, vol. 51, no. 31, pp. 863–867, 2018.

[53] X. Jin, Z. Li, N. V. Opinat Ikiela, X. He, Z. Wang, Y. Tao, and H. Lv, "An efficient trajectory planning approach for autonomous ground vehicles using improved artificial potential field," *Symmetry*, vol. 16, no. 106, pp. 1–17, 2024.

[54] Z. Pan, C. Zhang, Y. Xia, H. Xiong, and X. Shao, "An improved artificial potential field method for path planning and formation control of the multi-uav systems," *IEEE Transactions on Circuits and Systems-II: Express Briefs*, vol. 69, no. 3, pp. 1129–1133, 2022.

[55] J. Cenerini, M. W. Mehrez, J.-w. Han, S. Heon, and W. Melek, "Model predictive path following control without terminal constraints for holonomic mobile robots," *Control Engineering Practice*, vol. 132, 2023.

[56] P. Rangsichamras, N. Wittayaarereekul, S. Tantinarasak, I. Khuankrue, and C. Janya-anurak, "Cooperation of autonomous mobile robots with different maneuverability in transportation," *Society of Instrument and Control Engineers (SICE)*, pp. 187–192, 2023.

[57] G. Strang, *Linear Algebra and Its Applications*, 4th ed. Cengage Learning, 2011.

[58] R. C. Hibbeler, *Engineering Mechanics: Statics*, 13th ed. Pearson Prentice Hall, 2013, pp. 451–514.

[59] B. Braden, "The surveyor's area formula," *The College Mathematics Journal*, vol. 17, no. 4, pp. 326–337, 1986.

[60] W. Sun and Y.-X. Yuan, *Sequential Quadratic Programming*. Boston, MA: Springer US, 2006, pp. 523–560. [Online]. Available: https://doi.org/10.1007/0-387-24976-1_12

[61] T. Li, Y. Li, and Y. Qian, "Improved hungarian algorithm for assignment problems of serial-parallel systems," *Journal of Systems Engineering and Electronics*, vol. 27, no. 4, pp. 858–870, 2016.

[62] S. Kumar, T. Tawanda, E. Munapo, and P. Nyamugure, "A note on solving the transportation model by the hungarian method of assignment: Unification of the transportation and assignment models," *Intelligent Computing and Optimization*, pp. 301–313, 2023.

[63] H. W. Kuhn, "The hungarian method for the assignment problem," *Naval Research Logistics Quarterl*, vol. 2, no. 1-2, pp. 83–97, 1955.

[64] X. Fan, Y. Guo, H. Liu, B. Wei, and W. Lyu, "Improved artificial potential field method applied for auv path planning," *Mathematical Problems in Engineering*, 2020.

[65] Y. Liu, Y. Ren, J. Wang, L. Zhao, Q. Wang, and J. Shan, "Path planning for mobile robot based on improved artificial potential field method," *2023 China Automation Congress (CAC)*, pp. 4757–4762, 2023.